Journal of
Composites Science

MDPI

Article

Strength, Shrinkage and Early Age Characteristics of One-Part Alkali-Activated Binders with High-Calcium Industrial Wastes, Solid Reagents and Fibers

Dhruv Sood and Khandaker M. A. Hossain *

Department of Civil Engineering, Ryerson University, Toronto, ON M5B 2K3, Canada; dhruv.sood@ryerson.ca
* Correspondence: ahossain@ryerson.ca

Abstract: Alkali-activated binders (AABs) are developed using a dry mixing method under ambient curing incorporating powder-form reagents/activators and industrial waste-based supplementary cementitious materials (SCMs) as precursors. The effects of binary and ternary combinations/proportions of SCMs, two types of powder-form reagents, fundamental chemical ratios (SiO_2/Al_2O_3, Na_2O/SiO_2, CaO/SiO_2, and Na_2O/Al_2O_3), and incorporation of polyvinyl alcohol (PVA) fibers on fresh state and hardened characteristics of 16 AABs were investigated to assess their performance for finding suitable mix compositions. The mix composed of ternary SCM combination (25% fly-ash class C, 35% fly-ash class F, and 40% ground granulated blast furnace slag) with multi-component reagent combination (calcium hydroxide and sodium metasilicate = 1:2.5) was found to be the most optimum binder considering all properties with a 56 day compressive strength of 54 MPa. The addition of 2% v/v PVA fibers to binder compositions did not significantly impact the compressive strengths. However, it facilitated mitigating shrinkage/expansion strains through micro-confinement in both binary and ternary binders. This research bolsters the feasibility of producing ambient cured powder-based cement-free binders and fiber-reinforced, strain-hardening composites incorporating binary/ternary combinations of SCMs with desired fresh and hardened properties.

Keywords: alkali-activated binders; supplementary cementitious materials (SCMs); powder form reagents; precursors; fibers; shrinkage; microstructure

Citation: Sood, D.; Hossain, K.M.A. Strength, Shrinkage and Early Age Characteristics of One-Part Alkali-Activated Binders with High-Calcium Industrial Wastes, Solid Reagents and Fibers. *J. Compos. Sci.* **2021**, *5*, 315. https://doi.org/10.3390/jcs5120315

Academic Editor: Francesco Tornabene

Received: 14 October 2021
Accepted: 27 November 2021
Published: 30 November 2021

Highlights

- **Development of high calcium industrial wastes-based alkali-activated binders**
- **Use of dry mixing technique, powdered reagents, and ambient curing**
- **Evaluation of fresh state, strength, durability, and microstructural characteristics**
- **Influence of combinations/proportions of high calcium wastes and reagents evaluated**
- **Effect of micro-confinement created by fibers on compressive strength and shrinkage**

1. Introduction

Geopolymers are classified as alkali-activated materials (AAMs) produced from the activation of aluminosilicate-rich precursors by alkaline reagents [1]. The precursors were also found to be activated with phosphoric acid-based reagents in recent studies [2]. Precursors can be natural materials and industrial by-products such as fly ash (FA), ground granulated blast furnace slag (GGBFS), red mud, mine waste, and metakaolin [3]. The reactivity of these aluminosilicate sources depends on their chemical-mineralogical composition, morphology, fineness, and glassy phase content [4]. The main criteria for developing a stable geopolymer are that the source materials should be highly amorphous, possess sufficient reactive glassy content, have low water demand, and release aluminum easily. The alkaline activators such as sodium hydroxide (NaOH), potassium hydroxide (KOH), sodium silicate (Na_2SiO_3), and potassium silicate (K_2SiO_3) are used to activate the source materials by conventional two-part mixing technique. In a two-part technique, alkaline

reagent solutions and precursors/source materials are prepared separately and wet mixed to produce geopolymers. Geopolymerisation or alkali activation occurs when silicon and aluminum oxides react with alkaline reagents [5–8]. It is a mechanism that consists of the dissolution of various types of silica and aluminum from the surface of source materials, such as surface hydration of undissolved particles [5]. Polymerization occurs under highly alkaline conditions when reactive aluminosilicates are rapidly dissolved, and free [SiO_4]- and [AlO_4]-tetrahedral units are released in solution. The tetrahedral units are alternatively linked to polymeric precursors by sharing oxygen atoms, forming polymeric Si–O–Al–O bonds [1,9]. The development process of geopolymers uses 60% less energy and produces 80 to 90% fewer greenhouse gases than the synthesis of ordinary Portland cement (OPC)-based binders [7–11].

However, the factors involved in producing AAMs using the two-part mixing technique hinder its in situ applications. The geopolymers or alkali-activated binders (AABs) produced using conventional two-part technique require heat curing in most cases where low calcium precursors are incorporated to obtain satisfactory mechanical characteristics [7,8]. Therefore, the use of one part mixing technique incorporating a preblended dry mix of precursors (GGBFS and FA) and solid form reagents (sodium metasilicate and different grades of sodium silicates) was emphasized in recent studies [7,8,12–14]. The two-part mixing technique is an energy-intensive production process that reduces the commercial viability of geopolymers [13,14]. In addition, handling large quantities of solution-based alkaline reagents creates an undesirable environment for workers during construction applications [15–17]. Using a one-part mixing technique to produce AABs by just adding water (like cement-based binders) to the blended mix of precursors and solid/powder-based reagents can resolve issues associated with the two-part production technique. The powder form reagents can also be used in lesser quantities than their solution-based counterparts, thereby reducing the production cost of geopolymers [18,19]. The use of powdered reagents was found to facilitate the dissolution of silicate and aluminum ions from the precursors by increasing the pH of the fly ash/slag-based alkali-activated systems [20]. One-part geopolymer binders were produced by using precursors consisting of fly ash class F (FA-F), GGBFS, and hydrated lime with solid form reagents such as anhydrous sodium silicate and sodium hydroxide in previous research studies [21–24]. It was found that FA activation hydration products are zeolite type: sodium aluminosilicate hydrate or low calcium sodium aluminosilicate hydrate (N-A-S-H/N-C-A-S-H) gels with different Si/Al ratios. The primary binding phase produced in GGBFS activation is calcium silicate hydrate (C-S-H) or calcium aluminosilicate hydrate gel (C-A-S-H) with a low Ca/Si ratio, which is denser than the N-A-S-H gel and thus results in the refinement of the microstructure of combined GGBFS and FA incorporated mix compositions [21–24]. Although the physical properties of geopolymers prepared from various source materials/precursors may appear similar, their microstructures and chemical properties vary significantly [25,26]. In FA activation with sodium hydroxide (SH), the reaction starts with the dissolution of ions (Si and Al) from the precursors into the alkaline solution. Then, polymerization in the aluminum-rich first gel phase will transform into silica-rich final geopolymer gel [25,26]. When FA and metakaolin are compared, the reaction mechanisms seem similar in both materials [5]. However, under prevailing conditions, FA dissolution during geopolymerization is much slower than metakaolin [5]. The reaction mechanisms and products formed in the alkali activation of FA differ dramatically from those of the cement hydration. Therefore, the workability characteristics of alkali-activated FA binders should not be expected to be similar to cement-based binders [27]. In fly ash/slag-based geopolymer concrete mixes, higher drying shrinkage was associated with higher workability and lower compressive strength [25]. In addition, drying shrinkage strains were observed to proliferate at early ages and slowly diminish with time [25]. The alkali cations present in the binding gels (C-S-H/C-A-S-H) of alkali-activated slag cements have been found to create instability in their stacks and thus have facilitated the collapsing of these gels, leading to additional autogenous shrinkage in drying conditions [28]. Jeon et al. [29] reported that the formation

of ettringite in GGBFS-based geopolymer binders counteracts shrinkage in GGBFS-based geopolymer binders effectively [29]. Research on low-calcium FA and bottom ash-based geopolymer concrete, a part of the mixing water, was found to remain associated with the binding gels (N-A-S-H/N-C-A-S-H) [30]. The specimens made of such concrete lost free water and exhibited high drying shrinkage strains, especially during the initial two weeks when exposed to drying conditions (50% RH and 23 $\pm$ 2 °C) [30]. FA acting as a low reactive filler produced a dilution effect on GGBFS and resulted in lower drying shrinkage than the GGBFS alone or OPC mixes [31].

The geopolymer binders incorporating GGBFS as a precursor with solution-based reagents exhibited lower setting times than those made with powder form reagents [32]. The activation of GGBFS using sodium silicate (SS) solution resulted in fast-setting, owing to the development of C-S-H binding phases [33]. Increasing the mixing process time facilitated breaking of the initially formed C-S-H gels, enhanced workability, and improved mechanical characteristics of GGBFS-based binders [34]. The evolution of heat in alkali-activated GGBFS concrete was lower than OPC-based one [35]. The hydration heat in GGBFS concrete was still lower than OPC despite the increase in heat evolution with an increase in dosage and silica modulus of water glass (sodium silicate) [35]. The heat release pattern of alkali-activated GGBFS binder had also correlated with increased yield stress [36]. Incorporating calcium alumina cement (CAC) in pumice-type natural pozzolan-based geopolymer binders led to increased hydration heat. However, apparent activation energy was lower than the compositions without efflorescence control CAC [37]. The use of composite reagents (SS and sodium carbonate) facilitated in lowering the environmental impact and the associated costs with the use of single-component reagents (SS) [38]. The environmental sustainability of the one-part geopolymers using lower quantities of reagents and eliminating the need for heat curing was assessed to be more significant than their traditional two-part counterparts. The rate of dissolution of ions (Si and Al) from the precursors was different in the reaction processes of one-part and two-part geopolymers [39–41].

The literature review suggests a few studies on developing one-part AABs using high calcium precursors and calcium-based powder form reagents at ambient temperature using a dry mixing technique with adequate fresh state and hardened properties. Moreover, there is a scarcity of studies on shrinkage/expansion, mass change, and heat evolution characteristics of these binder systems. The effect of micro-confinement created by polyvinyl alcohol (PVA) fibers to inhibit shrinkage in AABs has not been studied extensively.

This paper presents the results of a research study to address the above-mentioned research gaps. The novel aspects of this paper include the use of binary/ternary proportions/combinations of high/low calcium industrial waste-based precursors, two combinations/dosages of the powder form calcium/sodium-based reagents, and PVA fibers for the development of AABs using one-part dry mixing technique established in authors previous studies [24,42]. The performance of developed one-part ambient cured binders is evaluated compared to conventional two-part heat-cured counterparts incorporating low calcium precursors and sodium-based reagents from previous research studies. The influence of the fundamental chemical ratios (SiO_2/Al_2O_3, Na_2O/SiO_2, CaO/SiO_2, and Na_2O/Al_2O_3) present in combinations of precursors and reagents on fresh state and hardened characteristics was investigated to characterize the performance of these binders. The effect of PVA fiber addition (2% v/v) on compressive strength, shrinkage/expansion, and mass change characteristics in two curing regimes (water and ambient/air) was also explored as novel aspect of the study. This research also contributes to the potential development of ready-mix AABs by incorporating dry powder-based mixing technology, eliminating the handling of a large quantity of corrosive solution-based reagents and heat curing. The findings of this paper can be used to facilitate the development and production of alkali-activated mortars, concretes, and fiber-incorporated composites for sustainable construction.

2. Experimental Program, Methods, and Materials

The experimental program consisted of a comprehensive performance evaluation of the developed 16 AAB compositions in terms of fresh state (workability, setting times, and time-dependent heat evolution), compressive strength (binders with and without fibers), durability (shrinkage/expansion and mass change of binders with and without fibers in water and ambient curing regimes), and microstructural (based on SEM/EDS and XRD analyses) characteristics.

2.1. Precursors of Alkali-Activated Binders

High calcium fly-ash class C (FA-C) with SiO_2+Al_2O_3+ $Fe_2O_3 \geq 50\%$; low calcium fly-ash class F (FA-F) with SiO_2+Al_2O_3+ $Fe_2O_3 \geq 70\%$; and ground granulated blast furnace slag (GGBFS) conforming to ASTM C618-2019 [43], ASTM C618-2019 [43], and ASTM C989-2018a [44] were used as source materials/precursors (aluminosilicate rich materials) for synthesizing AABs. The control binder mixes were developed using general use (type GU) cement and FA-F. The chemical compounds obtained through X-ray fluorescence spectrometer analysis, specific gravity (provided by the CRH, Mississauga, ON, Canada), and the Blaine fineness of the source materials are tabulated in Table 1. The particle size distribution of the supplementary cementitious materials (SCMs) and cement obtained through Malvern Mastersizer 2000 (Actlabs, Ancaster, ON, Canada) are presented in Figure 1.

Table 1. Chemical composition and physical properties of source materials and cement.

Chemical Compounds (%)	Fly Ash Class-C (FA-C)	Fly Ash Class-F (FA-F)	Ground Granulated Blast Furnace Slag (GGBFS)	Cement
SiO_2	36.53	55.66	35.97	19.35
Al_2O_3	18.26	22.09	9.18	5.31
Fe_2O_3	5.66	4.26	0.50	3.10
CaO	20.97	7.97	38.61	62
MgO	5.08	1.16	10.99	3
K_2O	0.68	1.49	0.36	-
Na_2O	4.04	4.10	0.28	0.23
MnO	0.03	0.03	0.25	-
TiO_2	1.26	0.61	0.39	-
P_2O_5	0.96	0.43	0.01	-
LOI.	2.18	1.05	0.74	2.40
Physical properties	FA-C	FA-F	GGBFS	Cement
Density (g/cm^3)	2.61	2.02	2.87	3.15
Retained on 45 μ, %		18		3
Blaine fineness (m^2/kg)	315	306	489.30	410

2.2. Reagents or Alkali Activators

This research study used two optimized types/combinations of powder-based reagents according to the authors' previous research [24]. The components of reagent 1 consisted of a combination of calcium hydroxide ($Ca(OH)_2$) and sodium meta-silicate ($Na_2SiO_3 \cdot 5H_2O$ with a modulus ratio of $SiO_2/Na_2O = 1$) in the ratio ($Ca(OH)_2/Na_2SiO_3 \cdot 5H_2O$) of 1:2.5. The components of the reagent 2 consisting of calcium hydroxide ($Ca(OH)_2$) and sodium sulfate (Na_2SO_4) were blended in the ratio ($Ca(OH)_2/Na_2SO_4$) of 2.5:1. The specific gravities of calcium hydroxide (pH = 12.4–12.6), sodium metasilicate (pH = 14), and sodium sulfate (pH = 7) were 2.24, 1.81, and 2.70, respectively. These reagents of lab-grade standard with a 95–100% purity were procured from National Silicates (Etobicoke, ON, Canada) and Westlab (Surrey, BC, Canada).

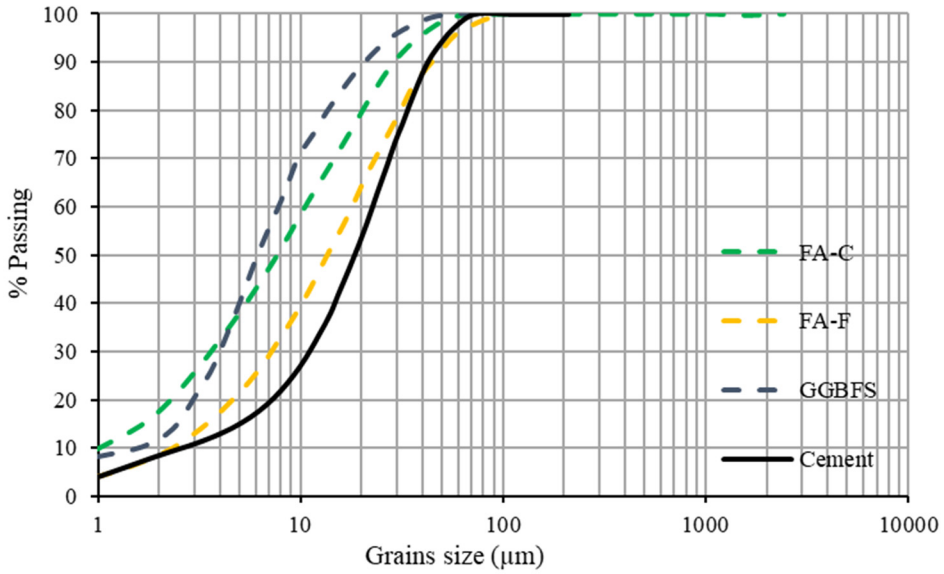

Figure 1. Particle size distribution of supplementary cementitious materials (SCMs) and cement.

2.3. Fibers and Superplasticizer

The specifications of the PVA fibers (PVA RECS 15) used to reinforce the binders provided by the supplier Nycon corporation (Fairless Hills, PA, USA) were as follows: length (8 mm), diameter (38 µm), Young's modulus (41 GPa), elongation (6.7%), density (1.3 g/cm^3), and tensile strength (1610 MPa).

A polycarboxylate ether-based superplasticizer (Adva Cast 575 from GCP applied technologies, Ajax, ON, Canada) with a pH of 6 was used to enhance the flowability of the mixes. This superplasticizer (SP) had a specific gravity of 1.06 g/cm^3 and approximately 40% solid content.

2.4. Mix Design and Specimen Preparation

Sixteen AAB mixes (eight with fiber and eight without fiber) were developed on the basis of the optimized mix compositions of reagent proportion/dosage (calcium hydroxide, sodium metasilicate, and sodium sulfate) and the proportion/combination of the precursors (FA-C, FA-F, and GGBFS) from the authors' previous study [24]. A paste based on a standard engineered cementitious composite (ECC) developed at Ryerson University was used as the control mix for this study [45,46]. The primary objective was to achieve fresh state and hardened characteristics of the AABs such as the paste component of ECC to assess their feasibility for producing cement-free PVA, fiber-reinforced, strain-hardening, alkali-activated composites in future studies. Table 2 presents the mix compositions of eight AABs without fiber. The other eight AABs had similar mix compositions but with the inclusion of 2% (v/v) of PVA fibers and designated by letter 'F' at the end of their mix designation separated by a hyphen. The mix compositions with and without fibers are separated by a comma in the mix designations presented in Table 2. The influence of incorporating PVA fibers (2% v/v) to the binder compositions on the shrinkage/expansion and mass change in two curing regimes was studied to see the effect of micro-confinement created by the fibers. The water to binder ratio varied from 0.35 to 0.375, while SP was kept fixed to 2% and 1% of the binder content for all the mix compositions with and without fibers. The two control (with and without fibers) binders (FP_C and FP_C-F) had a water to binder ratio of 0.27 and SP content of 0.06% and 1%. The mix designations and the chemical ratios present in the reagents and the precursors of 16 AABs and 2 control mixes (FP_C and FP_C-F) are presented in Table 2. The binary mixes designated as 'CS' are made of high-calcium FA-C and GGBFS, while ternary mixes designated as 'CFS' are made of high-calcium FA-C, low-calcium FA-F, and GGBFS combinations. The numeric value in mix designations denotes reagent types (type 1 and type 2), as explained earlier.

Table 2. Mix proportions for one-part binary and ternary binders with and without fiber.

Mix. Designation of Binders *	SCMs + P_C	P_C	SCM_S			R./B	Chemical Ratios (SCMs + Reagents)				28-Day Compressive Strength (MPa)
			FA-C	FA-F	GGBFS		SiO_2/Al_2O_3	Na_2O/SiO_2	CaO/SiO_2	Na_2O/Al_2O_3	
CS1, CS1-F	1	0	0.55	0	0.45	0.09	2.62	0.09	0.84	0.23	47.8, 45.2
CS1N, CS1N-F	1	0	0.50	0	0.50	0.09	2.71	0.08	0.87	0.23	41.5, 38.2
CFS1, CFS1-F	1	0	0.25	0.35	0.40	0.09	2.75	0.08	0.59	0.22	41.3, 38.6
CFS1N, CFS1N-F	1	0	0.25	0.25	0.50	0.09	2.86	0.07	0.69	0.21	38, 35.3
CS2, CS2-F	1	0	0.55	0	0.45	0.12	2.56	0.14	1.02	0.35	56.3, 53.1
CS2N, CS2N-F	1	0	0.50	0	0.50	0.12	2.64	0.13	1.02	0.35	43.4, 41.2
CFS2, CFS2-F	1	0	0.25	0.35	0.40	0.12	2.69	0.12	0.73	0.32	52.2, 49.8
CFS2N, CFS2N-F	1	0	0.25	0.25	0.50	0.12	2.80	0.12	0.84	0.33	39.1, 37.5
FP_C, FP_C-F	1	0.45	0	0.55	0	-	2.70	0.06	0.82	0.16	40.3, 38.1

All numbers are mass ratios of the binder. * Sixteen AABs + two control mixes without and with 2% (v/v) PVA fiber; binder denotes supplementary cementitious materials (SCMs) and Portland cement (P_C); C: FA-C, F: FA-F, S: GGBFS, N denotes mixes with an equal mass proportion of total FA and GGBFS; letter F in the mix designation after hyphen indicates fiber; the numeric value in mix designation denotes reagent types (type 1 and type 2).

The precursors and the reagents required for each mix composition (Table 2) were weighed and dry mixed for about 3 min in a shear mixer. After 3 min of dry mixing, two-thirds of the required water was gradually added to the mix. Then superplasticizer mixed with the remaining amount of water, which was gradually added for 2–3 min. PVA fibers were then added gradually (for mixes with PVA fiber) for 1–2 min, and mixing continued for another 2–3 min to avoid coagulation and facilitate uniform dispersion of the fibers. The total mixing time for mixes with and without fibers lasted for about 15–18 min and 10–13 min, respectively.

At least 12 cube specimens (50 mm × 50 mm × 50 mm) and eight prism specimens (25 mm × 25 mm × 285 mm) were prepared for each mix with and without fiber. The cube molds were placed in the curing room maintained at a temperature of 23 ± 3 °C and 95 ± 5% relative humidity (RH). The cubes were demolded after 24 h of casting and were kept in the curing chamber until the days of testing. The prism molds were stored and demolded according to the ASTM recommendations for drying shrinkage investigations.

2.5. Test Methods

All the tests were performed on mix compositions without fibers. Only shrinkage/expansion, mass change, and compressive strength investigations were conducted on both types of mixes (with and without fibers) to observe the effect of micro-confinement created by fibers in shrinkage mitigation and strength development. The compressive strength test at 7/14/28/56 days was conducted on three cube specimens (50 mm × 50 mm × 50 mm) per testing age for each mix composition according to ASTM C109/C109M [47]. The workability parameters of the mix compositions were assessed through a mini-slump cone test in compliance with ASTM C1437 [48]. The slump flow spread was measured, and the relative slump was evaluated on the basis of the following Equation (1) [49]:

$$T = \left[\left(\frac{d}{d_0}\right)^2\right] - 1 \quad (1)$$

where d = average of two measured diameters of the matrix spread and d_0 = bottom diameter of the conical cone (100 mm). The mixes without fibers were then tested for heat evolution for 72 h in compliance with ASTM C1753/C1753M [50]. The temperature increase/change was recorded with respect to time using a thermocouple wire inserted in the fresh binder mixes placed in Styrofoam containers. The containers were covered from the top to minimize the heat losses, as shown in Figure 2. The binders' initial and final setting time was determined as per ASTM C 191-a [51].

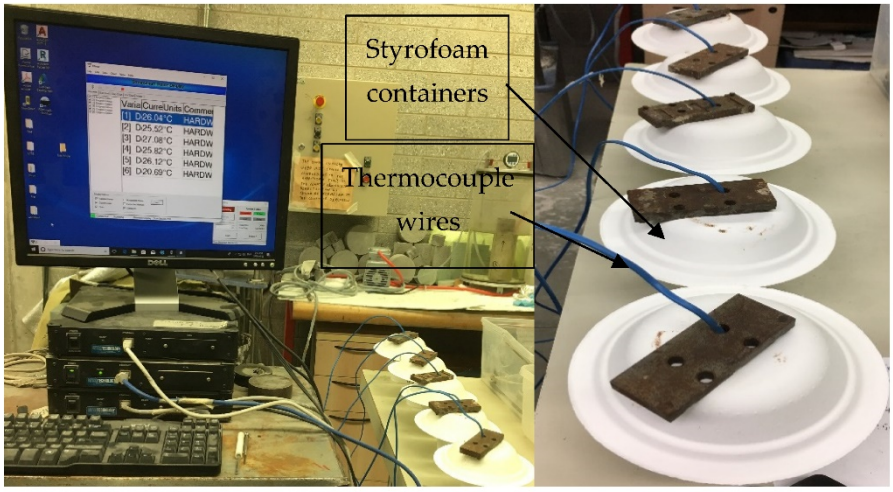

Figure 2. Test set-up for heat evolution.

The shrinkage/expansion test was conducted in compliance with ASTM standards [52–54] on both types of mixes (with and without fibers). Eight prismatic specimens with dimensions of 25 mm × 25 mm × 285 mm were prepared for each mix composition (with and without fibers) and de-molded after 24 h. The specimens were stored in airtight plastic bags until being de-molded. After demolding, initial mass and length readings were taken with a digital comparator with an accuracy of up to 0.001 mm and considered a reference. The length and mass change readings were taken at 1/7/28/56/90 days for the specimens in two curing regimes, water storage and air storage, in compliance with ASTM C157/157M [54]. In the water curing regime, specimens were kept immersed in water through the days of testing. For the air curing regime, after an initial curing period of 28 days in water immersion, four samples per mix composition were shifted to the drying room maintained at a relative humidity of 50 ± 4% and a temperature of 23 ± 2 °C, as shown in Figure 3a–c.

The SEM micrographs and EDS analysis were done on the best-performing alkali-activated binders and the control paste using JEOL 6380LV scanning electron microscope (SEM) equipped with energy dispersive X-ray spectroscopy (EDS). The specimens taken from the core of the failed compression test cubes at 28 days for SEM/EDS analysis were grounded and softly polished with sandpaper down to 30 µm. A gold coating was placed on the specimens to make the surface conductive. The fracture surface was studied using the secondary electrons (SE) and the backscattered electron (BES).

X-ray diffraction (XRD) analysis was conducted to determine the mineral phases in the binder mixes and validate the SEM/EDS results. The specimen preparation for performing XRD consisted of grounding the specimen taken from the core of the failed compression cubes. The grounded specimen was passed through a 200-mesh sieve. A Bruker D8 Endeavor diffractometer equipped with a Cu X-ray source and operating at 40 kV was used to identify the mineral phases using the PDF4/Minerals ICDD database.

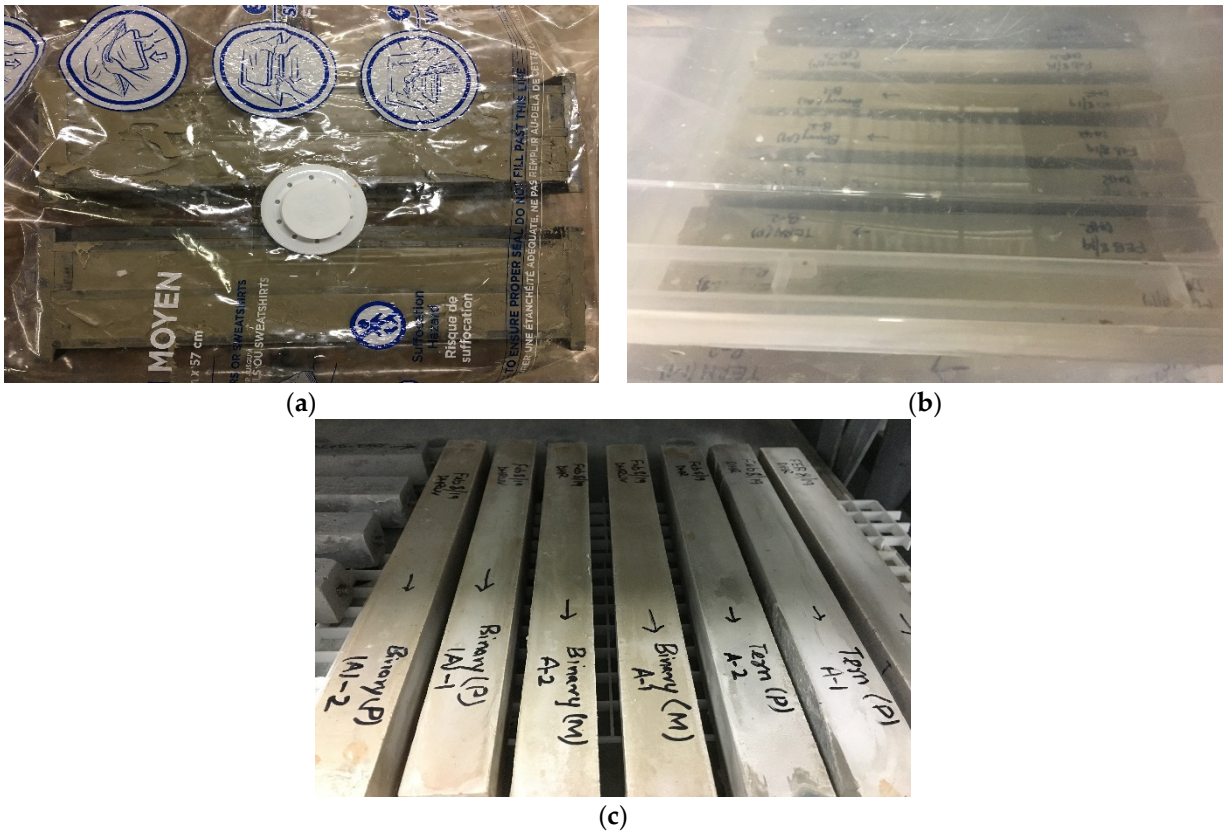

(**a**) (**b**) (**c**)

Figure 3. Curing regimes for drying shrinkage prisms: (**a**) airtight plastic bag storage for the first 24 h, (**b**) water storage, (**c**) air/ambient storage.

3. Results and Discussions

The performance of the developed binders (with and without fibers) is discussed in terms of fresh state (workability, setting time and heat evolution), compressive strength, durability (shrinkage/expansion and mass change in water and ambient curing regimes), and microstructural characteristics using SEM/EDS and XRD analysis.

3.1. Compressive Strength of Binders without and with Fibers Having Different Reagents

The binders without fibers (CS1, CS2, CFS1, and CFS2 with 55–60% FA + 40–45% GGBFS) incorporated with both reagents obtained 28 day compressive strengths ranging from 41 to 57 MPa (Table 2 and Figure 4a,b), while mixes (CS1N, CS2N, CFS1N, and CFS2N with 50% FA and 50% GGBFS) obtained 8% to 25% lower strength (38 to 43 MPa). Such lowering of compressive strength can be attributed to the presence of 5% to 10% higher GGBFS content that led to excessive calcium, which might have caused incompatibility or instability in the system. The compressive strength development was associated with the formation of both binding phases (C-A-S-H and N-A-S-H) in FA/GGBFS binders, as observed from the matrix microstructure through SEM/EDS and XRD analyses. The formation of such binding phases was also observed in previous research studies on FA/GGBFS-based alkali-activated mortars and composites [9,55–58]. The binders (without fibers) incorporating reagent 2 exhibited 2% to 18% higher 28 day compressive strength (between 39 and 57 MPa) than their reagent 1 counterparts (Figure 4a,b and Table 2) due to the formation of additional C-S-H gel formation associated with high calcium content in the system. This effect was more pronounced in binary binders due to their 5% higher GGBFS content, which led to more availability of Ca^{2+} ions for the formation of C-S-H and C-A-S-H binding phases, as revealed from the SEM/EDS and XRD investigations. Reagent 1 also produced binder mixes with compressive strength comparable to the control cement-based mix. These results are also consistent with the findings of previous research

works. The formation of the C-A-S-H binding phase produces high early and ultimate strength in high calcium binder and mortar systems [57–59].

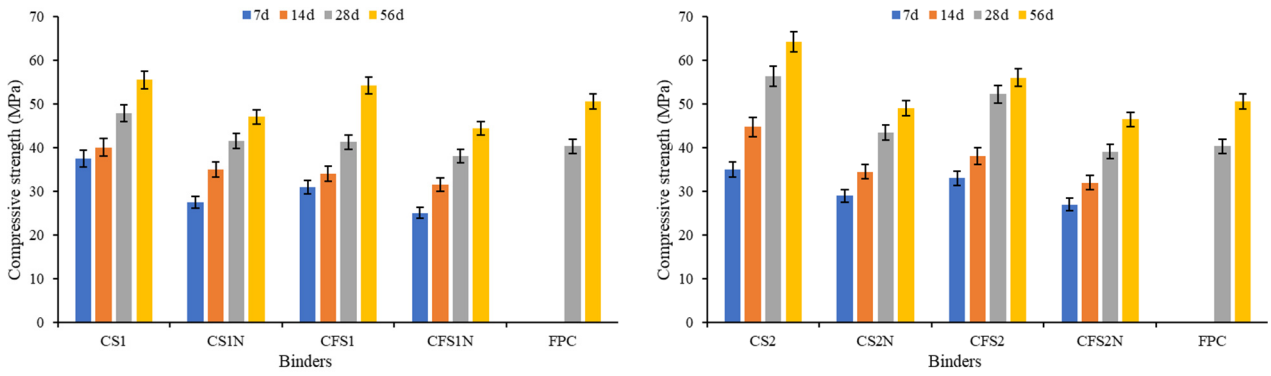

Figure 4. Compressive strength of binders with age: (**a**) influence of reagent 1, (**b**) influence of reagent 2.

The binary binders without fibers obtained compressive strengths ranging from 41 to 57 MPa at 28 days, as shown in Figure 4a,b. The formation of the C-A-S-H/C-S-H binding phase/gel in binary mixes was responsible for high early strength and faster strength gain, as verified from the SEM/EDS and XRD analysis and consistent with previous studies on fly-ash/GGBFS binders and mortars [57,58,60]. Ternary mixes obtained 7% to 14% lower strengths compared to binary binders at 28 days. This can be attributed to the relatively slow alkali activation process and the lower reactivity potential of FA-F. Both the binary and ternary mixes performed well compared to the control mix (FP_C) at 28 days, obtaining similar strength results at 56 days and exhibiting gradual strength gain with age.

The fiber-incorporated binders exhibited compressive strengths ranging from 35.3 to 53.1 MPa at 28 days, as noted in Table 2 and Figure 5. The fiber incorporation to the mixes can have two possible effects: firstly, an increase in porosity, and secondly, the control of crack opening [7,15,61,62]. The dominance of the first effect reduces the compressive strength, while the prevalence of the second effect can increase the compressive strengths by controlling the crack propagation or opening [7,15,61,62]. The fiber-reinforced binders obtained 1% to 8% lower or comparable compressive strengths compared to those without fibers (between 38 and 56.3 MPa) at 28 days (Table 2). This indicates that the phenomenon of porosity (air voids) addition to the mixes by the fibers was compensated by the fiber's intrinsic property of controlling the crack opening and propagation. This is consistent with previous research [14,15], where no significant improvements in compressive strengths were noted with the incorporation of fibers to the FA/GGBFS geopolymer mortar mixes. The slightly reduced strength of fiber-incorporated binders compared to their non-fiber counterparts can also be attributed to the possible balling of PVA fibers during mixing in small cube specimens used for determining compressive strength. The binders with (Figure 5) and without fibers (Figure 4) exhibited almost similar improvement in compressive strengths of 11% to 34% and 7% to 31%, respectively, from 28 to 56 days. The binders with and without fibers exhibited a standard deviation/error of up to ±5% in compressive strength, indicating their reliable consistency and repeatability characteristics.

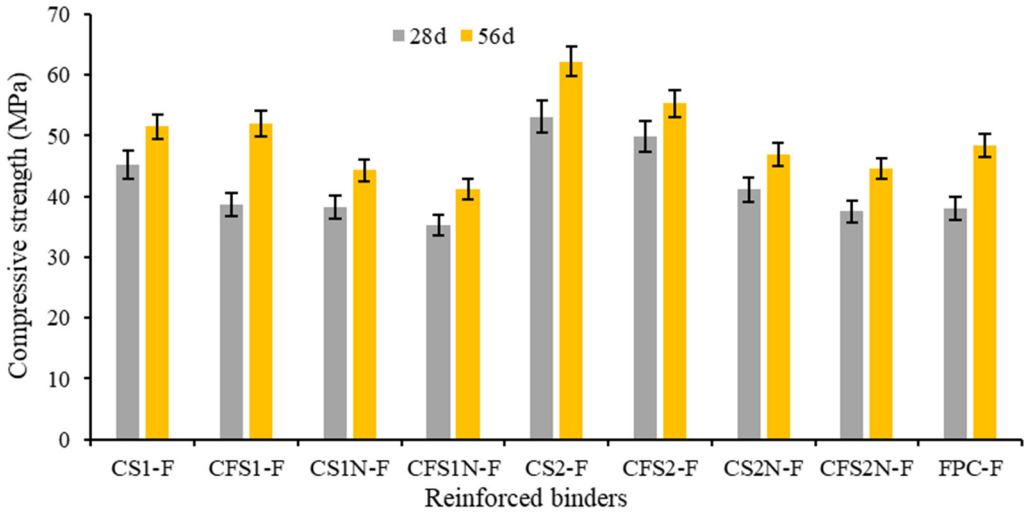

Figure 5. Compressive strength of binders with fibers (reinforced binders) at 28 and 56 days.

3.2. Workability of Binders

Figure 6a,b presents the slump flow spread and the relative slump of different binder mixes. The binder compositions (CS1, CS2, CFS1, and CFS2) exhibited a slump flow spread and relative slump varying from 165 to 230 mm and 1.7 to 4.3, respectively. Mix compositions (CS1N, CS2N, CFS1N, and CFS2N) obtained 2% to 6% lower slump flow spread and 6% to 16% lower relative slump than the former binder compositions. The mix compositions (CS1N, CS2N, CFS1N, and CFS2N) obtained a 2% to 29% lower slump flow spread and 5% to 61% lower relative slump than the control binder mix (FP_C), as depicted in Figure 6a,b. This can be attributed to 5–10% higher GGBFS content in these mixes. Higher calcium/GGBFS in the system resulted in a cement-like hydration process leading to the formation of C-A-S-H/C-S-H gel, as evident from SEM/EDS and XRD analysis. The dominant binding gel in a high calcium system was observed to be crystalline C-A-S-H under X-ray diffraction (XRD), which validates the workability parameters' results. Similar observations were made in a previous study on GGBFS-based binders and mortars incorporating CaO as a reagent [57,58,63]. The workability of the binders was not significantly affected by the incorporation of PVA fibers as normally observed in cement-based materials. This can be attributed to the release of water during geopolymerisation or alkali activation [20,39,40], whereas water is consumed during the hydration of cement-based materials. A low standard deviation of up to ±4.5% was seen in the companion mixes for the same mix composition indicating consistency in test results.

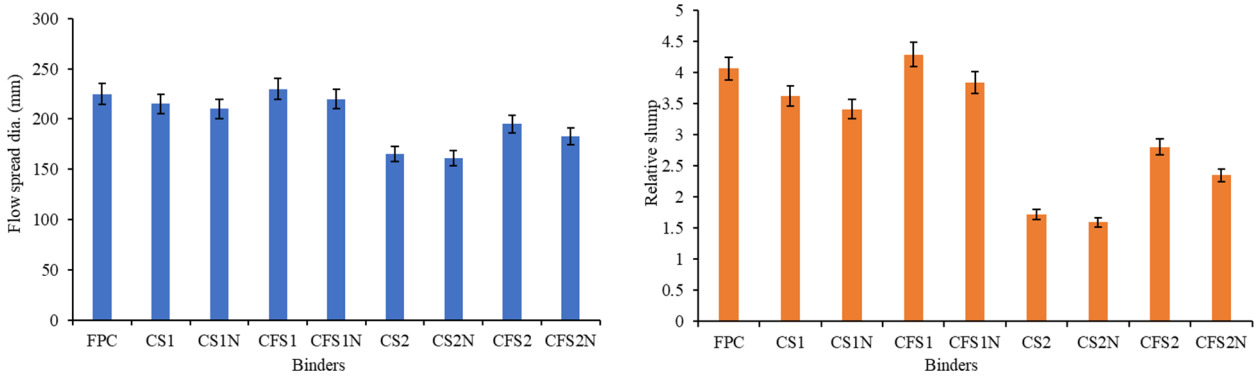

Figure 6. Workability characteristics of binders: (**a**) slump flow spread, (**b**) relative slump.

Reagent 1 effectively produced better flowable mixes, as shown in Figure 6a,b, leading to a slump flow spread of 210 to 230 mm for the binders (CS1, CS1N, CFS1, CFS1N). Hence, these binder mixes performed better, obtaining a 53% to 115% higher relative slump than other AABs. The high intrinsic alkalinity of sodium metasilicate (pH = 14) in these binder mixes resulted in a high degree of alkali activation, releasing water responsible for enhanced workability. Higher calcium content (calcium hydroxide/sodium sulfate = 2.5:1) in reagent 2 resulted in the formation of mainly C-A-S-H/C-S-H gels and comparatively less dissolution of silicate and aluminum ions responsible for geopolymerisation/alkali activation.

Ternary binders had better flowability (12% to 63% higher relative slump) than the binary mixes, as noted in Figure 6a,b. This was due to additional fly ash (class F) in the mix and 5% to 10% lower GGBFS content. Fly ash particles produce a ball-bearing-like effect due to their inherent round particles facilitating improved workability. Moreover, the presence of higher silicate and aluminate content in fly ash (class F), as indicated in Table 1, facilitates the release rate of 'Si' and 'Al' ions in the solution during geopolymerisation. This leads to more release of water in the system, which is responsible for improved workability. CFS1 also exhibited 6% superior performance than FP_C in terms of a relative slump due to the aforementioned reasons. A similar trend was reported in a previous study confirming the binary binders to be less workable than the ternary binders [57,64].

3.3. Heat Evolution of Binders

The binder mixes (CS1, CS2, CFS1, and CFS2) exhibited similar temperature–time curve profiles to their other corresponding binders (having total FA content equal to GGBFS content), as presented in Figure 7a,b, obtaining peak temperatures varying from 25 to 31 °C. The control mix (FP_C) obtained the highest peak temperature of 40 °C at 14 h. The binders (CS1, CS2, CFS1, and CFS2) obtained up to 7% lower peak temperatures than their corresponding AABs. Moreover, the time required to reach the peak temperatures was up to 15% higher in these mixes (CS1, CS2, CFS1, and CFS2), indicating a more gradual heat evolution process of such binders. This behavior can be attributed to lower GGBFS content (5 to 10%) in these mix compositions, which reduced the binder constituents' overall Blaine fineness. The temperatures for all the mixes became about the room/ambient temperature after 24 h of testing.

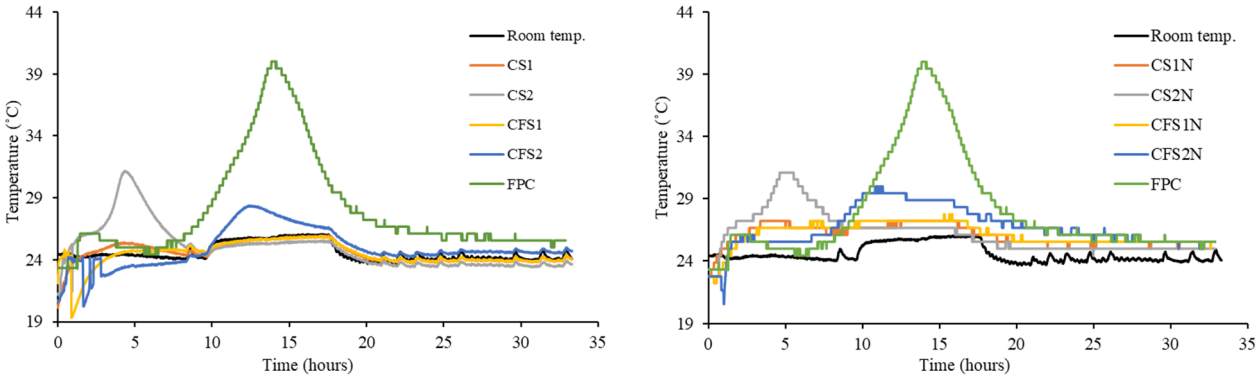

Figure 7. Evolution of temperature with time for binders: (**a**) FA (55% to 60%) + GGBFS (40% to 45%), (**b**) 50% FA + 50% GGBFS.

The peak temperatures for binders incorporating reagent 1 varied around the room/ambient temperature, as depicted in Figure 7a,b. The highest peak temperature of 27.7 °C was observed for CFS1N. The peak temperatures for binders with reagent 1 were 7% to 17% lower than those with reagent 2. The time required to reach the peak temperatures were 30% to 300% higher than the mix compositions with reagent 2. Thus, the temperature–time curves for these binders were more gradual, indicating a steadier heat evolution. The peak temperatures for binders with reagent 2 varied around 30 °C, with a maximum peak

temperature of 31 °C for CS2N. The higher peak temperatures for binders with reagent 2 can be attributed to the high calcium content ($Ca(OH)_2$:Na_2SO_4 = 2.5:1) of the reagent. This high calcium content is responsible for dominant cement hydration-like reaction, leading to higher peak temperatures, as observed for the control (FP_C) binder.

The binary and ternary binders with reagent 1 had similar temperature–time curve profiles, as noted in Figure 7a,b. However, the ternary binders with reagent 2 had 3% to 9% lower temperature peaks than their binary counterparts. Moreover, the time required to reach those temperature peaks was 140% to 185% higher than the binary mixes, indicating gradual heat evolution for such ternary mixes. This behavior can be attributed to 5% to 10% higher GGBFS content in the binary binders. The higher GGBFS/calcium content in the system leads to the formation of dominant C-A-S-H and C-S-H phases/gels responsible for higher heat evolution.

In general, the peak temperature was higher in binders with higher Ca content (maximum 31 °C) and control FPc with the highest Ca content developed the highest temperature of 40 °C. Previous research studies also confirmed such findings [35,36]. Fiber incorporation was also found to have little influence on the heat evolution of AABs.

3.4. Setting Time of Binders

The initial setting time of all binders ranged from 68 to 533 min, while the final setting ranged between 117 and 617 min. The binder CFS1N had the lowest initial and final setting times of 68 min and 117 min. Binders (CS1N, CS2N, CFS1N, and CFS2N) had 14% to 23% lower initial setting time and 21 to 40% lower final setting time than their counterpart AABs, as illustrated in Figure 8. The mix compositions (CS1N, CS2N, and CFS1N) had a 40% to 80% faster initial setting and 31 to 68% quicker final setting than the FP_C. This was because of 5% to 10% higher GGBFS content in these binders. Higher GGBFS/calcium content led to dominant calcium silicate hydrate binding phase/gel (C-S-H) in these binders, which utilized the water released in the geopolymeric/alkali activation process, leading to faster hardening. However, the ternary binder 'CFS2N' exhibited 25% and 31% higher initial and final setting times, respectively, than the control mix. This behavior can be attributed to a lower degree/rate of geopolymerisation in this mix due to the low alkalinity (pH: 7) of sodium sulphate. Standard deviations of up to ±7% and ±5% were seen in the initial and final setting times, indicating superior consistency in final setting times.

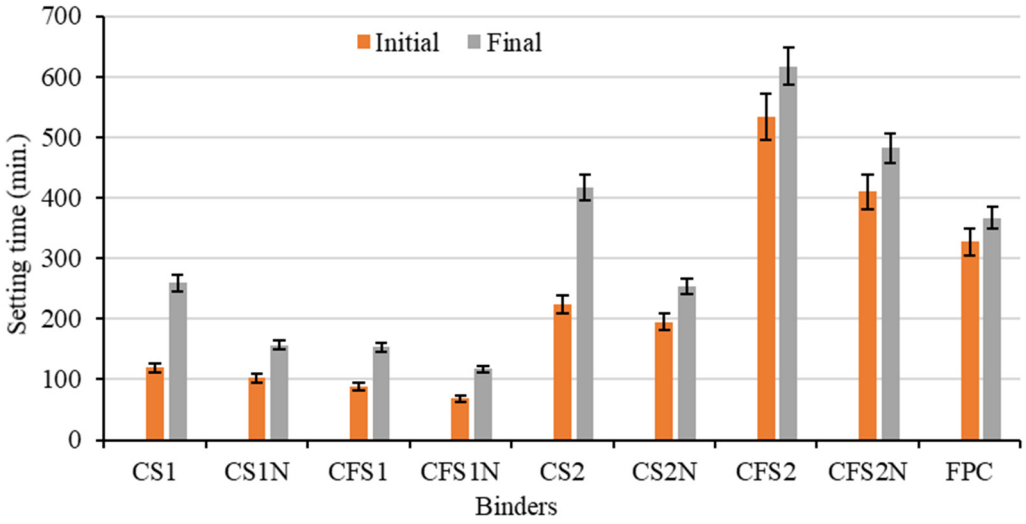

Figure 8. Initial and final setting times of binders.

Mix compositions (CS1, CS1N, CFS1, and CFS1N) had initial setting times varying from 68 to 120 min and final setting times ranging from 117 to 259 min. These binders exhibited 46% to 84% lower initial setting times and 37% to 76% lower final setting times than their counterparts (CS2, CS2N, CFS2, and CFS2N). Reagent 1 resulted in a higher

degree of geopolymeric/alkali activation reaction due to the enhanced ion dissolution potential of sodium metasilicate (SM) due to its characteristic higher alkalinity (pH 14). This led to the quicker setting of mixes incorporating reagent 1, as shown in Figure 8. Higher calcium content in reagent 2 led to the formation of C-S-H gel in addition to C-A-S-H. This might have resulted in incompatibility with the N-A-S-H gel formed because of geopolymerisation, which caused longer setting times.

Ternary binders with reagent 1 had 26% to 33% lower initial setting time and 25 to 41% lower final setting time than their binary counterparts. This trend can be attributed to higher silica and alumina content in fly ash (class F), which facilitated the ion dissolution process, leading to a higher degree of geopolymerisation. Ternary binders with reagent 2 had 110% to 138% longer initial setting time and 47% to 90% longer final setting time than their corresponding binary binders. The incompatibility between N-A-S-H gel and C-A-S-H/C-S-H gel formed because of higher calcium content in the system might have resulted in higher setting times. However, predominant C-A-S-H gel/binding phase formation in binary binders led to water consumption released in the geopolymeric process and a comparatively faster setting.

3.5. Shrinkage, Expansion, and Mass Change of Binders with and without Fibers

The shrinkage/expansion in any cementitious material is a vital durability property concerning its structural applications. The adverse shrinkage effects comprise micro-cracks and macro cracks or even breaking of structural elements due to the percolation of deleterious materials through the cracks. The length and mass change of unreinforced binders and binders reinforced with 2% v/v polyvinyl alcohol (PVA) fibers in water and air curing regimes are described in the following subsections:

3.5.1. Length Change of Unreinforced Binders in Water Curing Regime

The influence of binary and ternary combinations of SCMs on length change with age (1 to 90 days) in the water curing regime (solid line plots) is shown in Figure 9a,b. The control paste (FP_C) exhibited expansion until 28 days in water curing, followed by gradual shrinkage until the test completion (90 days). However, the length change remained positive, indicating it did not shrink more than its initial volume. This implies that the formation of reaction products, mainly CSH/C-A-S-H gels, resulted in expansion/swelling because of water consumption for the hydration process. The AAB mixes, however, exhibited shrinkage as they released water during the geopolymer/alkali activation reaction, as evident from Figure 9a,b and confirmed from earlier studies indicating the removal of unbound water from the hardened paste [56,65]. A higher shrinkage rate was observed during the first seven days, indicating the active formation of reaction products as seen in previous studies [66]. The length change in shrinkage became almost constant after 56 days for AAB mixes, indicating the completion of the alkali activation process. The mix compositions incorporating reagent 2 demonstrated relatively less shrinkage than the mixes with reagent 1, as depicted in Figure 9a,b. This can be attributed to fewer variations in reaction products/gels/binding phases, mainly of C-A-S-H/N(C)-A-S-H phases with traces of N-A-S-H in case of ternary mixes. Moreover, the high calcium content in the system due to the composition of reagent 2 resulted in the improved dissolution of fly ash. It enhanced the formation of reaction products, leading to the densification of the binder mixes and higher strength binders with reagent 2 compared to binders with reagent 1. The higher compressive strengths were seen to be associated with lower shrinkage strains in binders with reagent 2, and similar observations were made in previous investigations [25]. In the case of reagent 1, N-A-S-H binding phases were also observed in the SEM micrographs due to the system's high silica modulus responsible for releasing water during geopolymerisation.

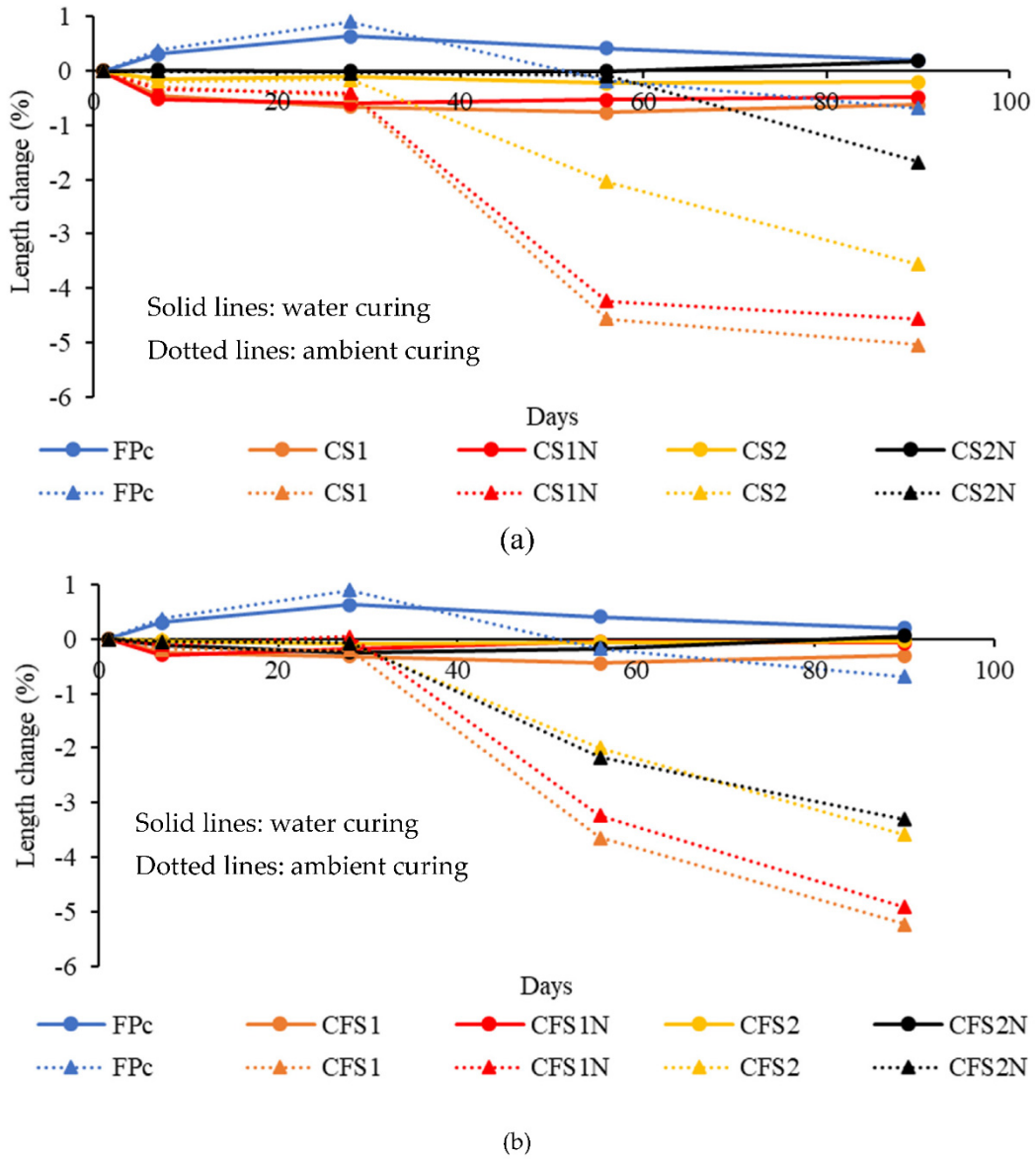

Figure 9. (**a**) Influence of the binary combinations of SCMs on length change. (**b**) Influence of the ternary combinations of SCMs on length change.

The ternary mixes showed lower shrinkage strains than their binary counterparts, as shown in Figure 9a,b. This can be due to FA-F's less reactive nature and the densification of resulting geopolymer gels (N-A-S-H/N(C)-A-S-H) by the cementitious binding phases. A similar trend was observed in earlier investigations where the incorporation of FA to GGBFS-based binders reduced shrinkage strains [67]. The C-A-S-H gels' dominant reaction product in binary binders exhibited viscous characteristics and a higher creep coefficient, resulting in higher deformation under the same load [68].

3.5.2. Length Change of Unreinforced Binders in Air Curing Regime

All the binder specimens suffered shrinkage after 28 days when shifted to the drying room, as indicated by dotted line plots in Figure 9a,b. However, the change in length (shrinkage) reduced after 56 days, meaning the near completion of the reaction process was observed for the specimens in ambient curing conditions. The binders incorporating reagent 1 demonstrated higher shrinkage strains (ranging from 3.24% to 4.56%) than their counterparts with reagent 2 (varying from 0.08% to 2.17%) at 56 days, as apparent from Figure 9a,b. Similar observations were made in previous studies on SCMs or natural

pozzolan (MK, FA, bottom ash, and pumice-type natural pozzolan)-based geopolymer binders [30,69,70], where shrinkage strains ranged from 2.5% to 3.25%, 1.25% to 2.35%, and 0.5% to 3% at 56, 70, and 90 days, respectively. This can be attributed to the formation of geopolymeric gels (N-A-S-H/N(C)-A-S-H) in these binders, including the binders with reagent 1 in the present study. These binding gels' formation resulted in the release of water during geopolymerisation, evaporating in ambient conditions. Moreover, possibly a part of mixing water present as interstitial water in these binding gels became evaporated in drying/ambient conditions, leading to high shrinkage strains. The shrinkage strains were relatively higher at 56 days in this present study compared to the previous studies because of the change in curing conditions (water curing to drying/ambient conditions) after 28 days to observe its implications on shrinkage and to account for realistic in situ curing periods. The binary binders exhibited up to 7% lower shrinkage strains than the ternary binders at 90 days, as depicted in Figure 9a,b, owing to the dominant formation of C-A-S-H gel, which is comparatively denser than the amorphous reaction products being formed in ternary binders. The exceptionally low shrinkage strain (1.67%) was reported for CS2N at 90 days because of the highest GGBFS content among all AABs, resulting in the additional formation of C-S-H gel with significant C-A-S-H binding phases.

3.5.3. Mass Change of Unreinforced Binders in Water Curing Regime

The effect of the binary and ternary combination of SCMs on mass change of specimens with age in water (solid line plots) and ambient (dotted line plots) curing regime is presented in Figure 10a,b. All mix compositions observed gradual mass gain with age. The mass change graph slope was steeper during the first seven days in water immersion, and it became almost constant after 28 days. The maximum positive mass change was observed for the control paste (FP_C) mixes of about 4.2%, as indicated in Figure 10a,b. There was a slight decrease in mass for CS1 and CFS1 during the initial seven days, marking the release of water during the formation of geopolymer products (N-A-S-H/N(C)-A-S-H).

The binder mixes with reagent 1 observed a slight decrease in mass at seven days due to the comparatively active formation of geopolymer products accompanied by water release. The binder CS2N reported the most significant mass change of about 2% at 28 days among all AAB mixes. This can be attributed to the formation of C-S-H gel in addition to the significant C-A-S-H binding phases. The binary and ternary binder mixes demonstrated similar mass change trends with age in water immersion, as shown in Figure 10a,b.

3.5.4. Mass Change of Unreinforced Binders in Air Curing Regime

The mass change followed the same trend as the binders exhibited for the change in length with age, as apparent from Figures 9a,b and 10a,b. There was a steep decline in mass for all binder specimens when the specimens were transferred to the drying room at 28 days. This was because the water released during geopolymerisation evaporated due to the drying conditions, resulting in mass reduction. The change in mass reduced after 56 days, indicating the near completion of the reaction process and the formation of reaction products resulting in the pore structure's refinement. A significant mass decline of up to 17.29% was observed for binder specimens with reagent 1 at 56 days, as indicated in Figure 10a,b. This can be attributed to sodium metasilicate's enhanced ion dissolution capability, which led to a higher degree of geopolymerisation, releasing water that became evaporated in drying conditions. The lowest mass change of 1.89% among AABs was noted for CS2N at 56 days due to the densification of the microstructure because of the formation of C-S-H gel in addition to the dominant C-A-S-H gel for binders with reagent 2.

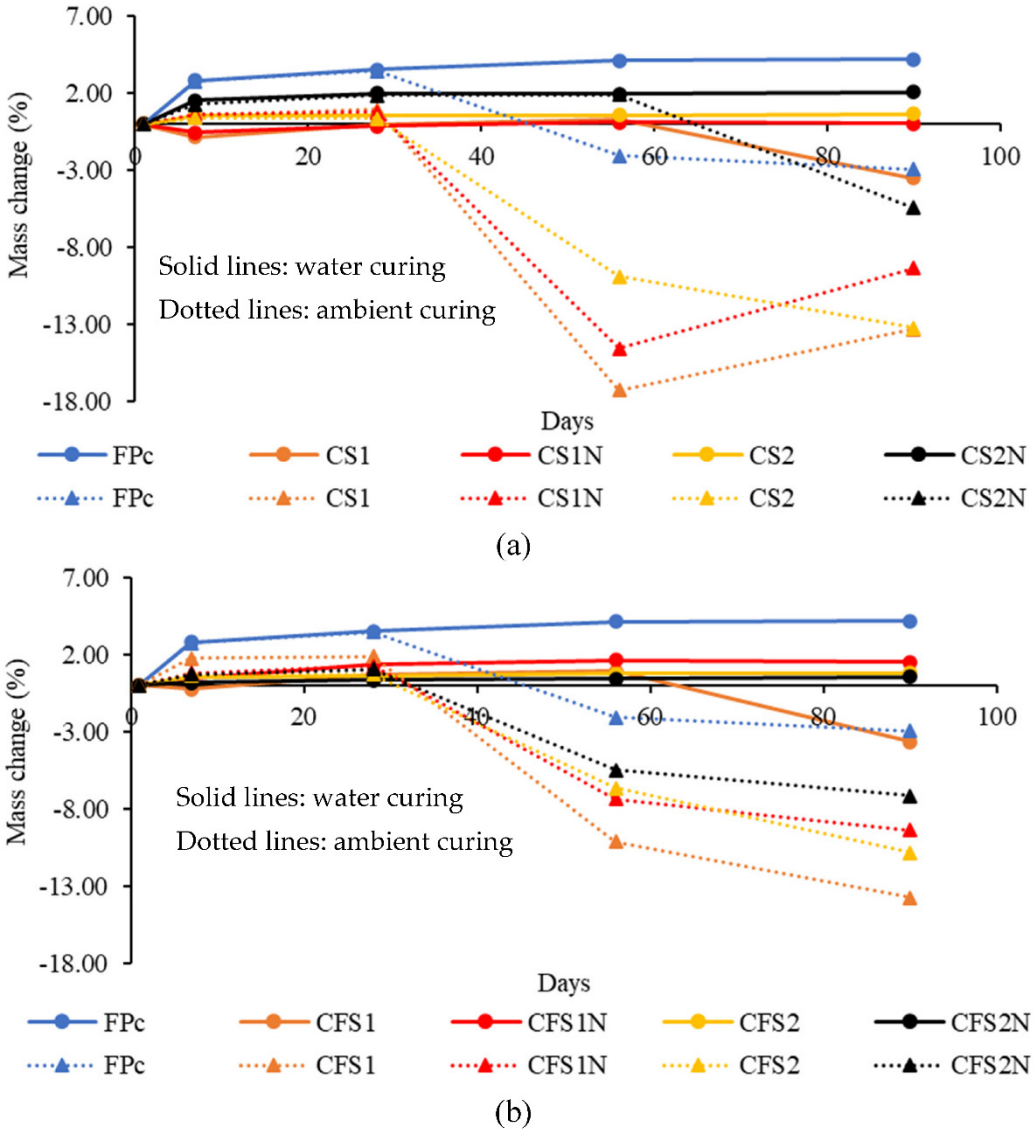

Figure 10. (**a**) Influence of the binary combinations of SCMs on mass change. (**b**) Influence of the ternary combinations of SCMs on mass change.

The ternary binders exhibited a lower change/decline in mass with age after 28 days compared to their binary counterparts, as presented in Figure 10a,b. This can be attributed to the densification of pore structure consisting of majorly N-A-S-H/N(C)-A-S-H gels in ternary binders with additional C-A-S-H binding phases resulting in a relatively lesser decline in mass.

3.5.5. Length Change of Binders with Fibers in Water Curing Regime

The influence of binary and ternary combinations of SCMs on the length change of binders reinforced with fibers with age (1 to 90 days) in the water (solid line plots) and ambient (dotted line plots) curing regime is demonstrated in Figure 11a,b. The comparison of length change at 56/90 days for binders with and without fibers in the water curing regime is tabulated in Table 3. The expansion was observed in all the reinforced binder (with fibers) specimens at all test intervals, contrary to the unreinforced binder (without fibers) specimens with an outlier mix CFS2N-F showing shrinkage at 90 days. A steep decrease in expansion was observed for all reinforced binders (with fibers) after 28 days, as shown in Figure 11a,b. The alkalis present in the pore solution acted as nucleation sites for the development of reaction products. The bonding of the reaction products with the

uniformly dispersed fibers, as shown in Figure 12a,b, facilitated in counteracting shrinkage in reinforced binders through micro-confinement. This active formation of reaction products until 28 days and the subsequent release of water during geopolymerisation can be considered as probable reasons for expansion.

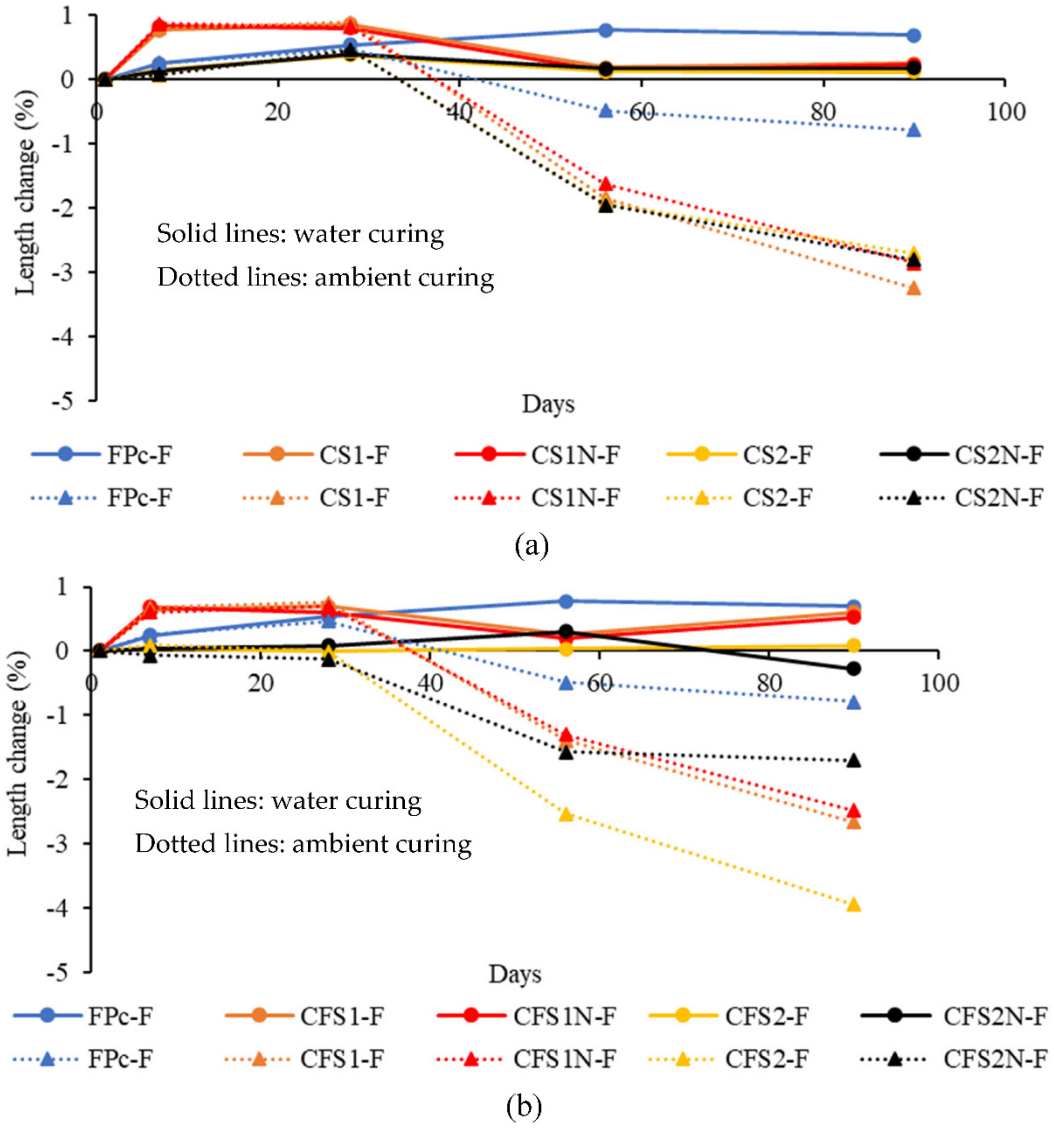

Figure 11. (**a**) Influence of binary combinations of SCMs in reinforced binders on length change. (**b**) Influence of ternary combinations of SCMs in reinforced binders on length change.

The length change in terms of expansion was more significant in reinforced binders incorporating reagent 1 than their counterparts with reagent 2, as depicted in Figure 11a,b. This could have been due to the predominant formation of N-A-S-H/N(C)-A-S-H binding phases in reinforced binders with reagent 1, resulting in the release of water subsequently absorbed by fibers. On the other hand, the development of mainly calcium-based crystalline reaction products in reinforced binders with reagent 2 led to water consumption for hydration and resulted in less expansion/swelling than amorphous products.

Table 3. Length and mass change of binders without and with fibers in water curing regime.

Binders—Unreinforced	Strain (%)		Mass Change (%)		Binders—Reinforced	Strain (%)		Mass Change (%)	
	56d	90d	56d	90d		56d	90d	56d	90d
FP_C	0.42	0.20	4.13	4.20	FP_C-F	0.77	0.69	3.09	3.25
CS1	−0.77	−0.63	0.26	−3.5	CS1-F	0.19	0.25	2.18	2.40
CS1N	−0.54	−0.48	0.12	0.02	CS1N-F	0.12	0.23	1.98	2.10
CS2	−0.22	−0.20	0.59	0.64	CS2-F	0.12	0.12	1.59	2.15
CS2N	0	0.18	1.95	2.05	CS2N-F	0.17	0.17	1.89	2.40
CFS1	−0.44	−0.30	0.93	−3.66	CFS1-F	0.27	0.60	1.42	1.69
CFS1N	−0.05	−0.06	1.66	1.53	CFS1N-F	0.20	0.52	0.96	1.36
CFS2	−0.06	−0.04	0.78	0.82	CFS2-F	0.03	0.08	2.62	2.66
CFS2N	−0.18	0.06	0.43	0.56	CFS2N-F	0.30	−0.27	1.22	1.46

Negative (−) sign in length and mass change indicates shrinkage and mass loss, and positive length and mass change denotes expansion and mass gain.

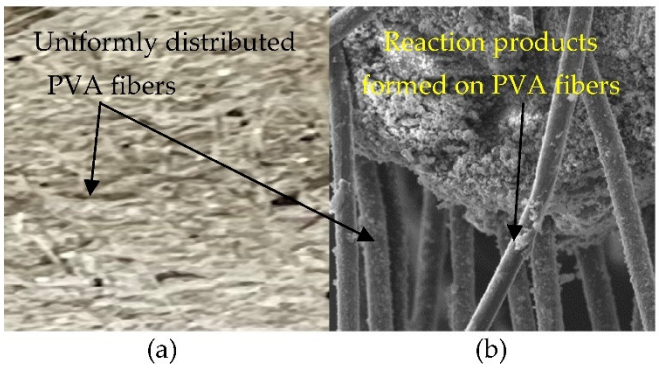

Figure 12. (**a**) Fracture surface showing uniformly distributed PVA fibers in the matrix. (**b**) Reaction products formed on the PVA fibers.

3.5.6. Length Change of Binders Reinforced with PVA Fibers in Air Curing Regime

The comparison of length change at 56/90 days for reinforced and unreinforced binders is tabulated in Table 4. The shrinkage strains for reinforced binders were within 0.48% for FP_C-F to 2.53% for CFS2-F at 56 days. In comparison, the shrinkage varied from 0.18% for FP_C to 4.56% for CS1 for unreinforced binders. This indicates that incorporating fibers into the binder mixes facilitated mitigating shrinkage, as apparent from Table 4 and validated by previous investigations on geopolymer binders reinforced with fibers [67]. The bridging action of the fibers and the formation of reaction products on the fibers made the reinforced binder system compact and denser.

Table 4. Length and mass change of binders without and with fibers in ambient curing regime.

Binder—Unreinforced	Strain (%)		Mass Change (%)		Binder—Reinforced	Strain (%)		Mass Change (%)	
	56d	90d	56d	90d		56d	90d	56d	90d
FP_C	−0.18	−0.69	−2.07	−2.94	FP_C-F	−0.48	−0.78	−0.71	−1.05
CS1	−4.56	−5.04	−17.29	−13.32	CS1-F	−1.84	−3.25	−4.21	−7.33
CS1N	−4.23	−4.56	−14.56	−9.36	CS1N-F	−1.62	−2.86	−2.46	−5.16
CS2	−2.04	−3.56	−9.92	−13.23	CS2-F	−1.92	−2.71	−4.66	−7.09
CS2N	−0.08	−1.67	1.89	−5.46	CS2N-F	−1.95	−2.80	−3.67	−6.24
CFS1	−3.64	−5.24	−10.12	−13.76	CFS1-F	−1.38	−2.66	−6.07	−8.99
CFS1N	−3.24	−4.91	−7.37	−9.38	CFS1N-F	−1.29	−2.48	−5.56	−6.96
CFS2	−2.00	−3.59	−6.67	−10.85	CFS2-F	−2.53	−3.94	−5.83	−9.74
CFS2N	−2.17	−3.30	−5.50	−7.14	CFS2N-F	−1.57	−1.70	−4.59	−5.93

Negative (−) sign in length and mass change indicates shrinkage and mass loss, and positive length and mass change denotes expansion and mass gain.

The reinforced binders with reagents 1 and 2 showed similar shrinkage behavior with age in drying conditions. CFS2-F observed maximum shrinkage strains of 2.53% at 56 days. The rate of length change declined after 56 days, as observed for un-reinforced binder specimens. There were slight variations in shrinkage strains with age for binary and ternary reinforced binders with reagent 1, as evident from Figure 11a,b.

3.5.7. Mass Change of Binders Reinforced with PVA Fibers in Water Curing Regime

The effect of binary and ternary combination of SCMs on mass change of reinforced binder specimens with age in water (solid line plots) and ambient (dotted line plots) curing regime is presented in Figure 13a,b. All the specimens exhibited a gradual mass gain, with the most significant gain during the initial seven days, suggesting the active formation of reaction products. The mass gain became almost constant after 56 days, indicating the completion of the alkali activation process and cementitious reactions as observed for unreinforced binder specimens, as noted in Table 3. The higher mass change was observed for all reinforced binders with few exceptions than their corresponding unreinforced binders. The formation of more reaction products on the uniformly distributed fibers and the water released during geopolymerisation might have been absorbed by the fibers. An increase in mass was observed with respect to initial mass (at 1 day) for all reinforced binders at all ages in water immersion, as indicated in Figure 13a,b.

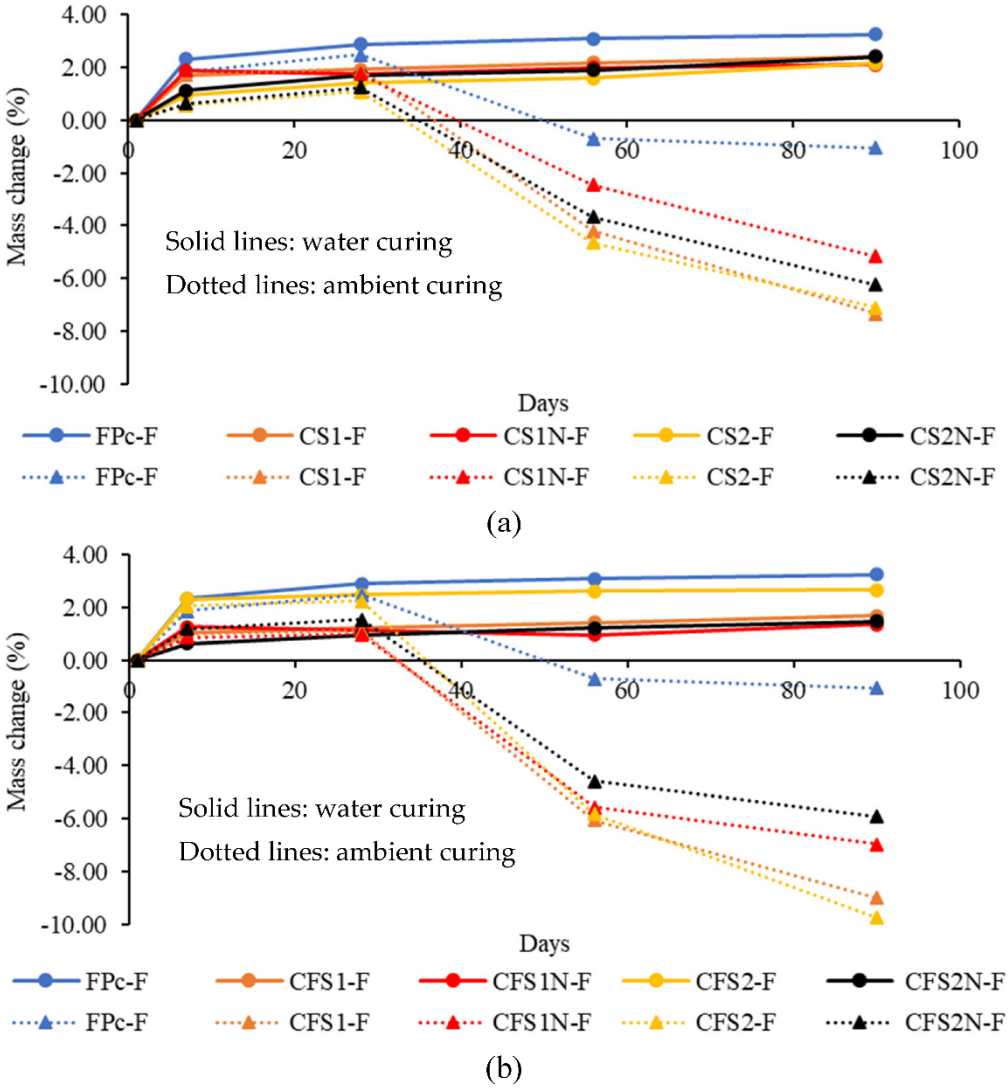

Figure 13. (**a**) Influence of the binary combinations of SCMs in reinforced binders on mass change. (**b**) Influence of the ternary combinations of SCMs in reinforced binders on mass change.

3.5.8. Mass Change of Binders Reinforced with PVA Fibers in Air Curing Regime

The mass decline with age of reinforced binder samples was contained within 0.71% for FP_C-F to 6.07% for CFS1-F at 56 days, as shown in Table 4. In comparison, the mass change for unreinforced binder specimens varied between +1.89% for CS2N and −17.29% for CS1 at 56 days. Incorporating fibers in the binders made them denser and more intact; therefore, less change in mass and volume with age was noted in drying conditions. Furthermore, the rate of change in mass declined after 56 days, indicating the near completion of the reaction process.

3.6. Microstructural Analysis

The morphology and microstructural characteristics of the binder/paste specimens were studied under a scanning electron microscope (SEM), and the elemental compositions of the reaction products were determined using energy-dispersive spectroscopy (EDS) analysis (Figures 14 and 15). The X-ray diffraction (XRD) analysis, as shown in Figure 16, was also performed to identify the mineral phases present in the binders and validate the SEM/EDS results.

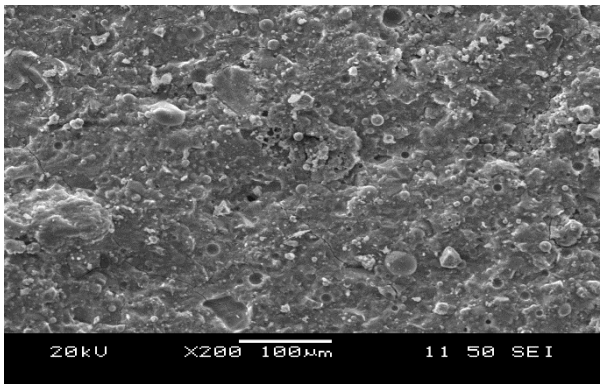

(**a**)

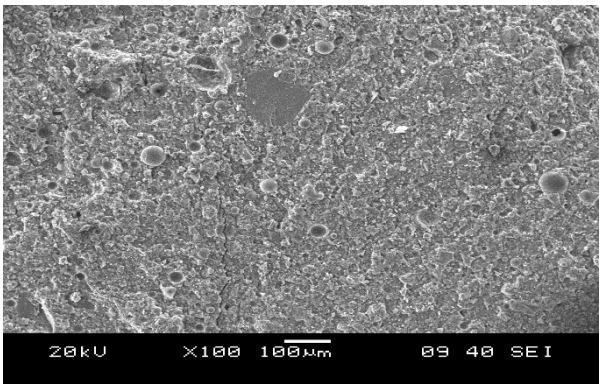

(**b**)

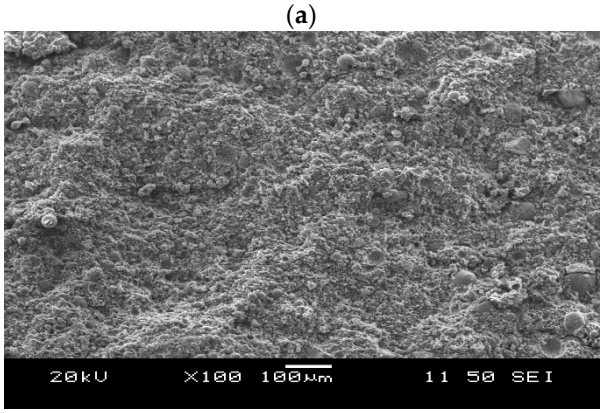

(**c**)

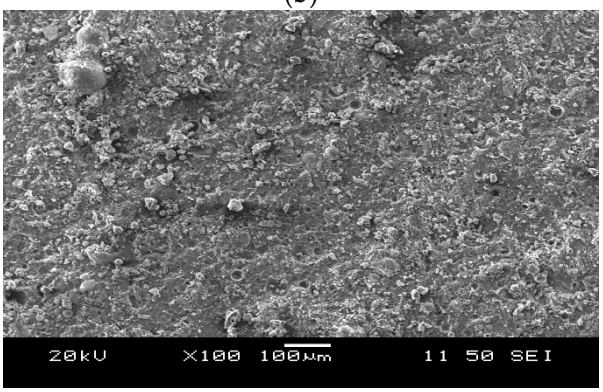

(**d**)

Figure 14. *Cont.*

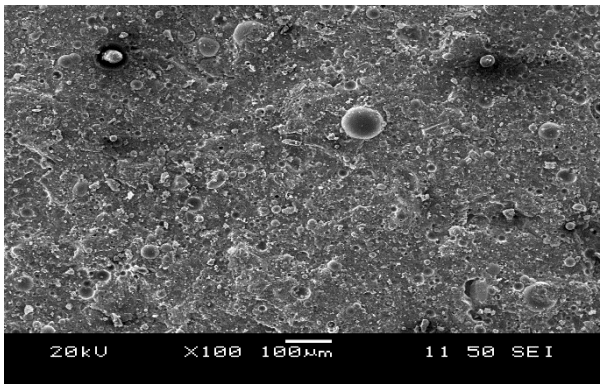

(**e**)

Figure 14. Morphology of binders at 28 days: (**a**) CS1, (**b**) CS2, (**c**) CFS1, (**d**) CFS2, (**e**) FP_C.

The morphology of the binary mix specimens (CS1 and CS2) illustrated in Figure 14a–d appeared to be partially amorphous, with significant portions of crystallized hexagonal plates, as identified from sharper peaks in the XRD analysis (Figure 16) compared to ternary counterparts (CFS1 and CFS2). The amorphous portion is associated with the geopolymerisation of fly ash (25%FA-C+35%FA-F), and crystalline plate-like structures are the reaction products of GGBFS. The binary binder CS2 obtained the highest 28 day compressive strength of 56.3 MPa and thus appeared to be the densest from the morphology depicted in Figure 14b. The ternary binder CFS2 was denser and had higher compressive strength than CFS1 due to a higher CaO/SiO_2 ratio because of higher calcium content in reagent 2. The high calcium in the system facilitated the dissolution of ions (silicate and aluminum) from the precursors [25]. The control mix FP_C showed a denser microstructure between binary and ternary AABs, attributed to the significant formation of C-S-H binding phases. Some partially/un-hydrated grains of fly ash (FA-F) and cement can be seen embedded in the matrix in Figure 14e.

The micrograph (Figure 15a) of the binary binder (CS1) indicated C-A-S-H gel as the main reaction product from EDS and XRD analysis. Moreover, small traces of amorphous N-C-A-S-H were formed, owing to the composition of reagent 1. Similar binding phases or gels (C-A-S-H) were predominantly characterized in earlier microstructural investigations on FA and GGBFS-based alkali-activated binders [9]. The crystallized plate-like structure formed in the SEM micrograph having compounds with high aluminum content (C_4AlH_{13}), also confirmed from EDS analysis (Al: 7.2%), was due to the presence of GGBFS in the binder composition. The binary binder CS2 showed the formation of mainly C-A-S-H and C-S-H binding phases (with C_4AlH_{13} compound having a lower aluminum content of 3.6%) due to the higher calcium content in the system, owing to the composition of reagent 2 (Figure 15b). Similar binding phases/gels were characterized in recent studies on fly ash and slag-based pastes/mortars [57,58,71]. This additional C-S-H gel formation further densified the microstructure and improved compressive strength compared to binder CS1. Figure 15a,b shows some un-hydrated/partially hydrated particles of both GGBFS, as well as FA-C embedded in both the matrices (CS1 and CS2).

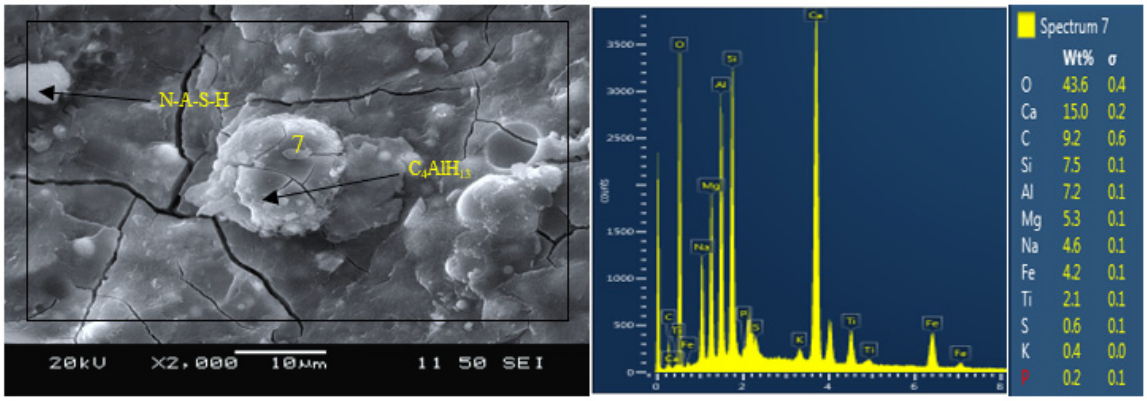

(**a**)

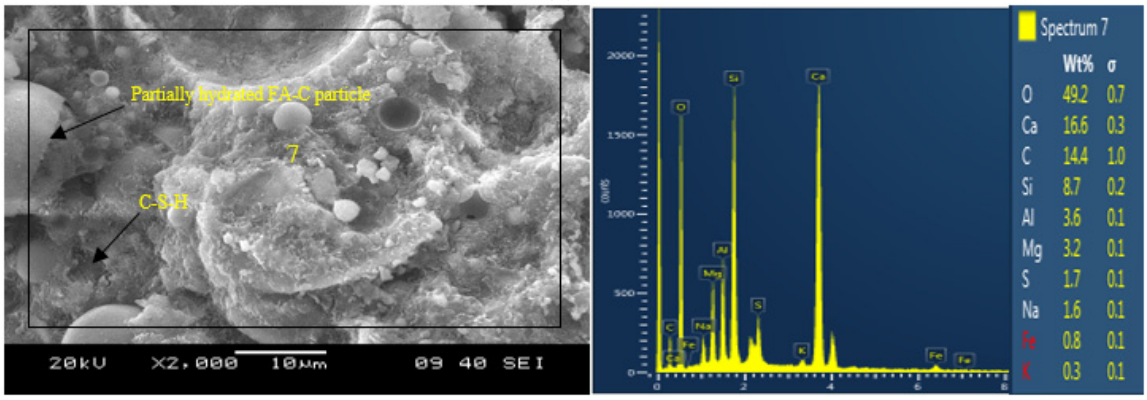

(**b**)

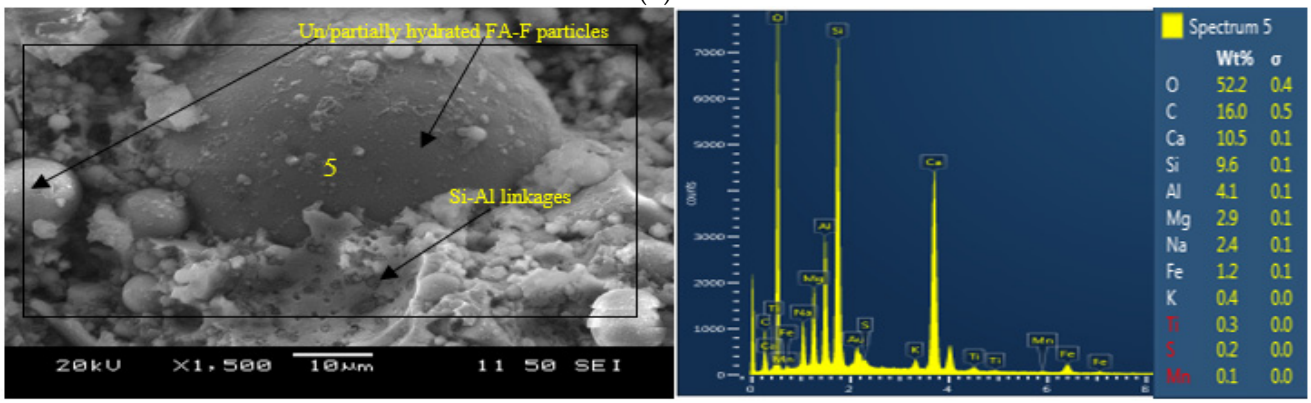

(**c**)

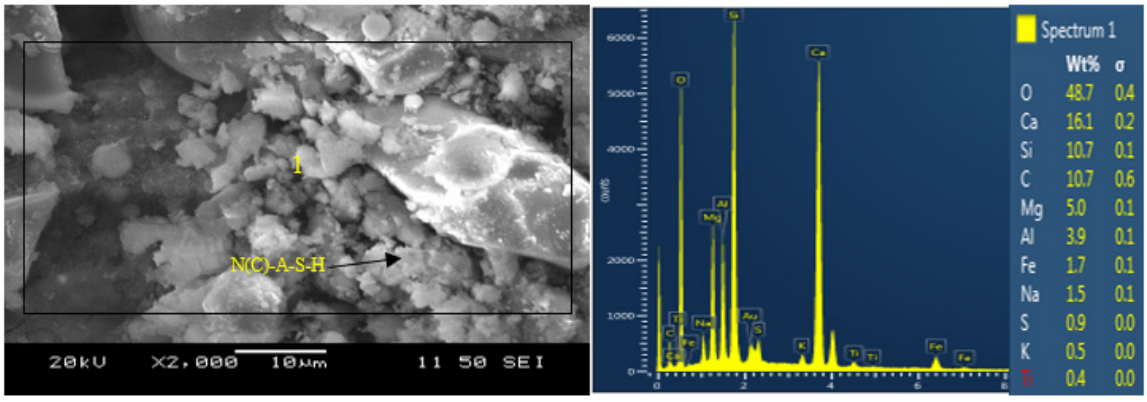

(**d**)

Figure 15. *Cont.*

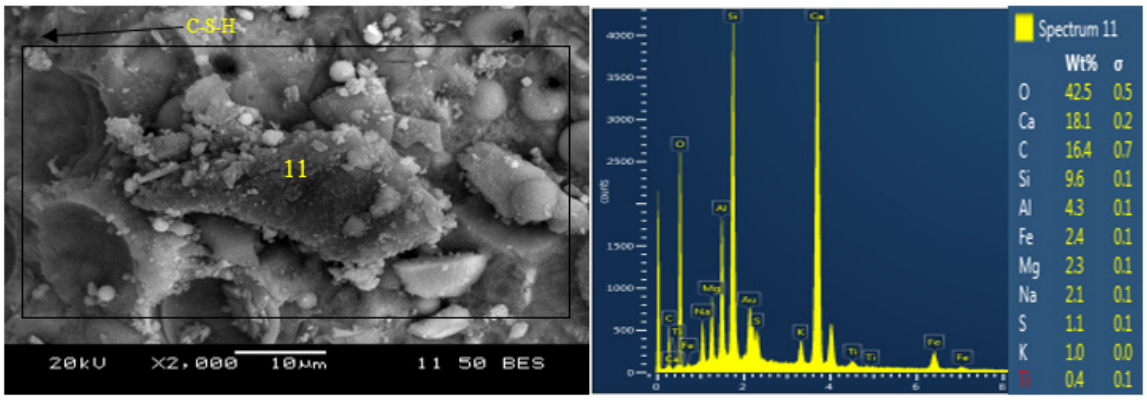

(**e**)

Figure 15. (**a**) SEM micrographs and EDS analysis of the binary binder CS1. (**b**) SEM micrographs and EDS analysis of the binary binder CS2. (**c**) SEM micrographs and EDS analysis of the ternary binder CFS1. (**d**) SEM micrographs and EDS analysis of the ternary binder CFS2. (**e**) SEM micrographs and EDS analysis of the control cement binder FP_C.

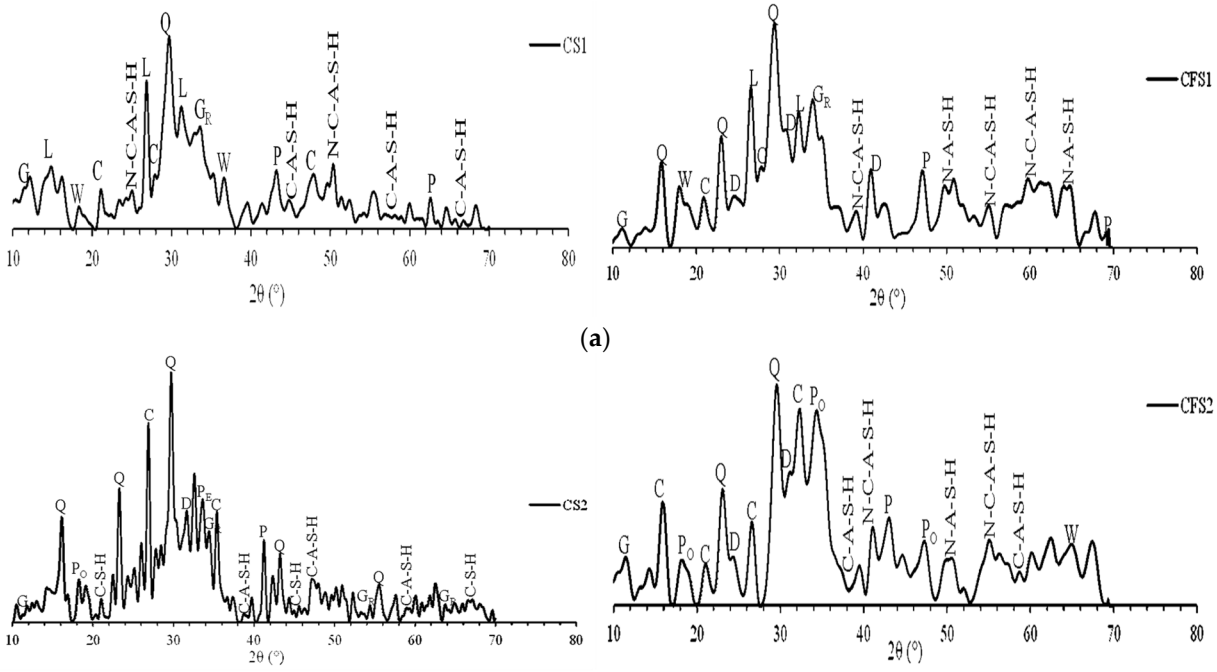

(**a**)

(**b**)

Figure 16. XRD patterns: (**a**) CS1 and CFS1, (**b**) CS2 and CFS2 (Q-quartz, G-gypsum, D-dolomite, G_R-grossular, P_o-portlandite, P-periclase, L-lalondeite, C-calcite, W-wadalite).

Ternary binders (CFS1 and CFS2) obtained lower strengths than binary binders (CS1 and CS2), owing to the larger particle size of FA-F. Hence, the most significant amount of un-hydrated/partially hydrated fly ash (FA-F) was seen in the CFS1 micrograph shown in Figure 15c, owing to its low reactivity because of the presence of firm chains Si–Al that needed to be broken first to initiate the reaction process. These un-hydrated particles of FA-F acted as inert particles and resulted in comparatively lower strengths than their binary counterparts. The primary reaction products for ternary binder CFS1 (with reagent 1) consisted of low calcium N(C)-A-S-H and N-A-S-H gels with Si–Al linkages, while N(C)-A-S-H, N-A-S-H, and C-A-S-H gels were formed for CFS2 (with reagent 2) as indicated in SEM/EDS and XRD analyses (Figures 15c,d and 16a,b). The availability of higher Ca^{2+} ions from reagent 2 ($Ca(OH)_2$:Na_2SO_4 = 2.5:1) and FA-F with high intrinsic silica content led to the additional formation of C-S-H and C-A-S-H gels in CFS2 binders. The formation of these

extra binding phases resulted in the refinement of pore structure, leading to higher strength of binder CFS2 compared to its CFS1 counterpart. The building of such gel products were characterized by the elements Ca, Al, Si, and Na in EDS analyses (Figure 15c,d).

The reaction products in the control paste (FP_C) mainly consisted of C-S-H gels (Figure 15e) because of the cement hydration (high content of calcium and silica in cement) and the pozzolanic reaction of FA-F (high content of silica and alumina in FA-F suitable for pozzolanic reactions) without alkaline reagents. While for AABs, the process of alkali activation or geopolymerisation facilitated by alkaline reagents led to the formation of crystalline (C-A-S-H with traces of C-S-H) and amorphous (N-C-A-S-H and N-A-S-H) products, as shown in Figure 15a,d.

The XRD diffractograms of the binary and ternary paste mix incorporating reagents 1 and 2 with their identified mineral phases are presented in Figure 16a,b. The principal mineral phases were quartz, calcite, and dolomite for mixes with reagent 2, showing a higher number of peaks than their counterparts with reagent 1. The binding phases of C-A-S-H and N-C-A-S-H were identified as the primary reaction products because of their higher intensities and presence in the diffractograms of binders CS2 and CFS2 than the other binding phases and noted earlier in the SEM/EDS analysis. Moreover, some phases of Portlandite were seen in binders with reagent 2, indicating excessive calcium in the system. The highest peak representing quartz for CS1, CS2, CFS1, and CFS2 was identified at 29.7° 2θ. A combination of binding gels consisting of N-A-S-H or N-C-A-S-H and C-A-S-H, as determined earlier in SEM/EDS analysis, were observed to have higher intensities and presence in the diffractograms of CFS1 and CS1. The dominant mineral phases consisting of lalondeite, grossular, quartz, and calcite were observed from 26° 2θ to 38° 2θ in the diffractograms of CFS1 and CS1 as presented in Figure 16a,b. Few traces of periclase (MgO) and gypsum were present in all the binders. The presence of gypsum counteracted the quick setting of mixes, and MgO content in the compositions is known for inhibiting shrinkage by its characteristic expansive nature [45]. The diffractograms of binary binders (CS1 and CS2) exhibited more and sharper peaks than their ternary counterparts (CFS1 and CFS2), representing the formation of more crystalline products.

4. Conclusions

Sixteen binary and ternary alkali-activated binders (AABs) without and with 2% polyvinyl alcohol (PVA) fibers were developed from the optimum combinations/proportions of precursors such as fly ash class C (FA-C), fly ash class F (FA-F), and ground granulated blast furnace slag (GGBFS) incorporating powder-based reagents (reagent 1: calcium hydroxide + sodium metasilicate and reagent 2: calcium hydroxide + sodium sulfate). The performance of the developed binary (FA-C + GGBFS) and ternary (FA-C + FA-F + GGBFS) binders was discussed in terms of their fresh state, mechanical, durability, and microstructural characteristics. The following conclusions are drawn from this study:

- Binary and ternary binders without fibers with 40% to 45% GGBFS content demonstrated 8% to 34% higher compressive strengths than their counterparts (having 50% FA and 50% GGBFS), irrespective of the type of reagent. The use of GGBFS more than 45% had the adverse effect of reducing the compressive strength of the binders. There seemed to be a threshold of calcium content in the system, as a 5% to 10% increase in the proportion of GGBFS in binary and ternary binders resulted in an 8% to 25% reduction of compressive strength. GGBFS content of 45% in the binder mix compositions was found to be the optimum, according to strength characteristics.
- The fiber incorporation did not play a significant role in the compressive strength development as the binders with and without fibers obtained comparable strength at 28 and 56 days. The effect of additional porosity created by the fibers was balanced by the fiber bridging action controlling crack opening and propagation.
- The binary and ternary mixes without fibers having a GGBFS content of 50% exhibited a 6% to 16% lower relative slump than their counterpart AABs. Ternary binder 'CFS1' composed of 25% FA-C, 35% FA-F, and 40% GGBFS with reagent 1 obtained the

highest slump flow spread of 230 mm and the highest relative slump of 4.3, achieving a 56-days compressive strength of 54 MPa.

- The primary binding phases/gels in binary binders are a combination of C-A-S-H and C-S-H, as noted in SEM/EDS and XRD analyses. A combination of N-A-S-H or low calcium N(C)-A-S-H and C-A-S-H gels were the reaction products for ternary binders. The binders with reagent 2 generally produced higher compressive strength compared to their reagent 1 counterparts due to the presence of Portlandite, leading to the formation of additional C-S-H gel. The presence of sharper crystalline peaks in XRD consisting mainly of quartz and calcite for binders incorporating reagent 2 also supported the development of higher compressive strengths.
- A wide range of initial (68 to 533 min) and final (117 to 617 min) setting times were obtained for binary and ternary binders without fibers. Binders, both binary and ternary, having a GGBFS content of 50%, exhibited 14% to 23% lower initial and 21% to 40% lower final setting times than other AABs.
- Ternary binders without fibers demonstrated lower shrinkage strains (varying from 0.036% to 0.296% at 90 days) compared to their binary counterparts (ranging from 0.20% to 0.628%) in water immersion because the un-hydrated FA-F particles acted as inert material filling the voids as well as continuous supplying of released water during alkali activation. The formation of reaction products on the fibers with subsequent micro-confinement created by the fibers by bridging action and resisting crack opening in binary/ternary binders facilitated shrinkage mitigation.
- The binary and ternary binders without fibers having 40% to 45% GGBFS content incorporating reagents 1 and 2 were found to have better performance in terms of higher workability and gradual time-dependent heat evolution (peak temperatures between 25 °C and 31 °C), with lower heat of hydration (minimizing early age shrinkage cracks) and higher compressive strength.
- This study confirms the feasibility and commercial viability of producing sustainable binary/ternary green alkali-activated binders and composites using industrial wastes with satisfactory properties using a dry mixing method under ambient curing. PVA fiber-incorporated binders can also be used to develop alkali-activated engineered cementitious composites with strain-hardening and micro-cracking characteristics.

Author Contributions: Conceptualization, D.S. and K.M.A.H.; formal analysis, D.S.; funding acquisition, K.M.A.H.; investigation, D.S. and K.M.A.H.; methodology, D.S. and K.M.A.H.; project administration, K.M.A.H.; resources, K.M.A.H.; supervision, K.M.A.H.; writing—original draft, D.S. and K.M.A.H.; writing—review and editing, K.M.A.H. All authors have read and agreed to the published version of the manuscript.

Funding: This research was funded by Natural Sciences and Engineering Research Council (NSERC) Canada, grant number RGPIN-5613-2019.

Institutional Review Board Statement: Not applicable.

Informed Consent Statement: Not applicable.

Conflicts of Interest: The authors declare no conflict of interest.

References

1. Davidovits, J. Geopolymers Inorganic polymeric new materials. *J. Therm. Anal.* **1991**, *37*, 1633–1656. [CrossRef]
2. Krishna, R.S.; Mishra, J.; Zribi, M.; Adeniyi, F.; Saha, S.; Baklouti, S.; Uddin, F.; Shaikh, A.; Gokce, H.S. A review on developments of environmentally friendly geopolymer technology. *Materialia* **2021**, *20*, 101212. [CrossRef]
3. Slaty, F.; Khoury, H.; Wastiels, J.; Rahier, H. Characterization of alkali activated kaolinitic clay. *Appl. Clay Sci.* **2013**, *75*, 120–125. [CrossRef]
4. Xu, H.; Deventer, J.S.J.V. The geopolymerisation of alumino-silicate minerals. *Int. J. Miner. Process.* **2000**, *59*, 247–266. [CrossRef]
5. Görhan, G.; Aslaner, R.; Sinik, O. The effect of curing on the properties of metakaolin and fly ash-based geopolymer paste. *Compos. Part. B Eng.* **2016**, *97*, 329–335. [CrossRef]
6. Duxson, P.; Fernandez-Jime, A.A.; Provis, A.J.L.; Lukey, G.C.; Palomo, A.A.; Deventer, J.S.J.V. Geopolymer technology: The current state of the art. *J. Mater. Sci.* **2006**, *42*, 2917–2933. [CrossRef]

7. Shah, S.F.A.; Chen, B.; Oderji, S.Y.; Aminul, M.H.; Ahmad, M.R. Comparative study on the effect of fiber type and content on the performance of one-part alkali-activated mortar. *Constr. Build. Mater.* **2020**, *243*, 118221. [CrossRef]
8. Farasat, S.; Shah, A.; Chen, B.; Yousefi, S.; Haque, M.A.; Riaz, M. Improvement of early strength of fly ash-slag based one-part alkali activated mortar. *Constr. Build. Mater.* **2020**, *246*, 118533.
9. Wei, X.; Ming, F.; Li, D.; Chen, L.; Liu, Y. Influence of water content on mechanical strength and microstructure of alkali-activated Fly Ash/GGBFS mortars cured at cold and polar regions. *Materials* **2020**, *13*, 138. [CrossRef]
10. Samantasinghar, S.; Singh, S.P. Fresh and Hardened Properties of Fly Ash–Slag Blended Geopolymer Paste and Mortar. *Int. J. Concr. Struct. Mater.* **2019**, *13*, 47. [CrossRef]
11. Nematollahi, B.; Sanjayan, J.; Uddin, F.; Shaikh, A. Ceramics International Synthesis of heat and ambient cured one-part geopolymer mixes with different grades of sodium silicate. *Ceram. Int.* **2015**, *41*, 5696–5704. [CrossRef]
12. Ding, Y.; Shi, C.J.; Li, N. Fracture properties of slag/fly ash-based geopolymer concrete cured in ambient temperature. *Constr. Build. Mater.* **2018**, *190*, 787–795. [CrossRef]
13. Bong, S.H.; Nematollahi, B.; Nazari, A.; Xia, M.; Sanjayan, J. Efficiency of Different Superplasticizers and Retarders on Properties of "One-Part" Fly Ash-Slag Blended Geopolymers with Different Activators. *Materials* **2019**, *12*, 3410. [CrossRef] [PubMed]
14. Nematollahi, B.; Sanjayan, J.; Qiu, J.; Yang, E.H. High ductile behavior of a polyethylene fiber-reinforced one-part geopolymer composite: A micromechanics-based investigation. *Arch. Civ. Mech. Eng.* **2017**, *17*, 555–563. [CrossRef]
15. Abdollahnejad, Z.; Mastali, M.; Falah, M.; Shaad, K.M.; Luukkonen, T.; Illikainen, M. Durability of the Reinforced One-Part Alkali-Activated Slag Mortars with Different Fibers. *Waste Biomass Valoriz.* **2021**, *12*, 487–501. [CrossRef]
16. Alrefaei, Y.; Wang, Y.S.; Dai, J.G. The effectiveness of different superplasticizers in ambient cured one-part alkali activated pastes. *Cem. Concr. Compos.* **2019**, *97*, 166–174. [CrossRef]
17. Luukkonen, T.; Sreenivasan, H.; Abdollahnejad, Z.; Yliniemi, J.; Kantola, A.; Telkki, V.V.; Kinnunen, P.; Illikainen, M. Influence of sodium silicate powder silica modulus for mechanical and chemical properties of dry-mix alkali-activated slag mortar. *Constr. Build. Mater.* **2020**, *233*, 117354. [CrossRef]
18. Nematollahi, B.; Sanjayan, J.; Qiu, J.; Yang, E.-H. Micromechanics-based investigation of a sustainable ambient temperature cured one-part strain hardening geopolymer composite. *Constr. Build. Mater.* **2017**, *131*, 552–563. [CrossRef]
19. Alrefaei, Y.; Dai, J.G. Tensile behavior and microstructure of hybrid fiber ambient cured one-part engineered geopolymer composites. *Constr. Build. Mater.* **2018**, *184*, 419–431. [CrossRef]
20. Provis, J.L. Alkali-activated materials. *Cem. Concr. Res.* **2018**, *114*, 40–48. [CrossRef]
21. Chi, M. Effects of dosage of alkali-activated solution and curing conditions on the properties and durability of alkali-activated slag concrete. *Constr. Build. Mater.* **2012**, *35*, 240–245. [CrossRef]
22. Dong, M.; Elchalakani, M.; Karrech, A. Development of high strength one-part geopolymer mortar using sodium metasilicate. *Constr. Build. Mater.* **2020**, *236*, 117611. [CrossRef]
23. Deb, P.S.; Nath, P.; Sarker, P.K. The effects of ground granulated blast-furnace slag blending with fly ash and activator content on the workability and strength properties of geopolymer concrete cured at ambient temperature. *Mater. Des.* **2014**, *62*, 32–39. [CrossRef]
24. Sood, D.; Hossain, K.M.A. Optimizing Precursors and Reagents for the Development of Alkali-Activated Binders in Ambient Curing Conditions. *J. Compos. Sci.* **2021**, *5*, 59. [CrossRef]
25. Neupane, K.; Kidd, P.; Chalmers, D.; Baweja, D.; Shrestha, R. Investigation on compressive strength development and drying shrinkage of ambient cured powder-activated geopolymer concretes. *Aust. J. Civ. Eng.* **2016**, *14*, 72–83. [CrossRef]
26. Singh, B.; Gupta, M.; Bhattacharyya, S. Geopolymer concrete: A review of some recent developments. *Constr. Build. Mater.* **2015**, *85*, 78–90. [CrossRef]
27. Lee, W.K.W.; Deventer, J.S.J.V. Effects of Anions on the Formation of Aluminosilicate Gel in Geopolymers. *Ind. Eng. Chem. Res.* **2002**, *41*, 4550–4558. [CrossRef]
28. Neto, A.A.M.; Cincotto, M.A.; Repette, W. Drying and autogenous shrinkage of pastes and mortars with activated slag cement. *Cem. Concr. Res.* **2008**, *38*, 565–574. [CrossRef]
29. Jeon, I.K.; Ryou, J.S.; Jakhrani, S.H. Effects of Light-Burnt Dolomite Incorporation on the Setting, Strength, and Drying Shrinkage of One-Part Alkali-Activated Slag Cement. *Materials* **2019**, *12*, 2874. [CrossRef]
30. Xie, T.; Ozbakkaloglu, T. Behavior of low-calcium fly and bottom ash-based geopolymer concrete cured at ambient temperature. *Ceram. Int.* **2015**, *41*, 5945–5958. [CrossRef]
31. Zhu, Y.; Yang, Y.; Yao, Y. Use of slag to improve mechanical properties of engineered cementitious composites (ECCs) with high volumes of fly ash. *Constr. Build. Mater.* **2012**, *36*, 1076–1081. [CrossRef]
32. Yang, K.H.; Song, J.K.; Ashour, A.F.; Lee, E.T. Properties of cementless mortars activated by sodium silicate. *Constr. Build. Mater.* **2008**, *22*, 1981–1989. [CrossRef]
33. Puertas, F.; Varga, C.; Alonso, M.M. Rheology of alkali-activated slag pastes. Effect of the nature and concentration of the activating solution. *Cem. Concr. Compos.* **2014**, *53*, 279–288. [CrossRef]
34. Palacios, M.; Banfill, P.F.G.; Puertas, F. Rheology and setting of alkali-activated slag pastes and mortars: Effect if organic admixture. *ACI Mater. J.* **2008**, *105*, 140–148.
35. Awoyera, P.; Adesina, A. A critical review on application of alkali activated slag as a sustainable composite binder. *Case Stud. Constr. Mater.* **2019**, *11*, e00268. [CrossRef]

36. Puertas, F.; Gonz Alez-Fonteboa, B.; Gonz Alez-Taboada, I.; Alonso, M.M.; Torres-Carrasco, M.; Rojo, G.; Martínez-Abella, F. Alkali-activated slag concrete: Fresh and hardened behaviour. *Cem. Concr. Compos.* **2018**, *85*, 22–31. [CrossRef]
37. Kani, E.N.; Allahverdi, A.; Provis, J.L. Calorimetric study of geopolymer binders based on natural pozzolan. *J. Therm. Anal. Calorim.* **2017**, *127*, 2181–2190. [CrossRef]
38. Ma, C.; Zhao, B.; Guo, S.; Long, G.; Xie, Y. Properties and characterization of green one-part geopolymer activated by composite activators. *J. Clean. Prod.* **2019**, *220*, 188–199. [CrossRef]
39. Luukkonen, T.; Abdollahnejada, Z.; Yliniemia, J.; Kinnunena, P.; Illikainen, M. One-part alkali-activated materials: A review. *Cem. Concr. Res.* **2017**, *103*, 21–34. [CrossRef]
40. Abdollahnejad, Z.; Luukkonen, T.; Mastali, M.; Giosue, C.; Favoni, O.; Ruello, M.L.; Kinnunen, P.; Illikainen, M. Microstructural Analysis and Strength Development of One-Part Alkali-Activated Slag/Ceramic Binders Under Different Curing Regimes. *Waste Biomass Valoriz.* **2020**, *11*, 3081–3096. [CrossRef]
41. Luukkonen, T.; Abdollahnejad, Z.; Yliniemi, J.; Kinnunen, P.; Illikainen, M. Comparison of alkali and silica sources in one-part alkali-activated blast furnace slag mortar. *J. Clean. Prod.* **2018**, *187*, 171–179. [CrossRef]
42. Sood, D.; Hossain, K.M.A.; Manzur, T.; Hasan, M.J. Developing Geopolymer Pastes Using Dry Mixing Technique. In Proceedings of the 7th International Conference on Engineering Mechanics and Materials (CSCE 2019), Laval, QC, Canada, 12–15 June 2019; pp. 1–8.
43. ASTM C618. *Standard Specification for Coal Fly Ash and Raw or Calcined Natural Pozzolan for Use in Concrete*; ASTM International: West Conshohocken, PA, USA, 2019.
44. ASTM C989/C989M. *Standard Specification for Slag Cement for Use in Concrete and Mortars*; ASTM International: West Conshohocken, PA, USA, 2018.
45. Sherir, M.A.; Hossain, K.M.A.; Lachemi, M. Self-healing and expansion characteristics of cementitious composites with high volume fly ash and MgO-type expansive agent. *Constr. Build. Mater.* **2016**, *127*, 80–92. [CrossRef]
46. Sherir, M.A.; Hossain, K.M.A.; Lachemi, M. Permeation and Transport Properties of Self-Healed Cementitious Composite Produced with MgO Expansive Agent. *J. Mater. Civ. Eng.* **2018**, *30*, 04018291. [CrossRef]
47. ASTM C109/C109M. *Standard Test Method for Compressive Strength of Hydraulic Cement Mortars (Using 2-in. or [50-mm] Cube Specimens)*; ASTM International: West Conshohocken, PA, USA, 2016.
48. ASTM C1437. *Standard Test Method for Flow of Hydraulic Cement Mortar*; ASTM International: West Conshohocken, PA, USA, 2015.
49. Nematollahi, B.; Sanjayan, J. Effect of different superplasticizers and activator combinations on workability and strength of fly ash based geopolymer. *Mater. Des.* **2014**, *57*, 667–672. [CrossRef]
50. ASTM C1753/C1753M. *Standard Practice for Evaluating Early Hydration of Hydraulic Cementitious Mixtures Using Thermal Measurements*; ASTM International: West Conshohocken, PA, USA, 2015.
51. ASTM C191. *Standard Test Methods for Time of Setting of Hydraulic Cement by Vicat Needle*; ASTM International: West Conshohocken, PA, USA, 2018.
52. ASTM C490/C490M. *Standard Practice for Use of Apparatus for the Determination of Length Change of Hardened Cement Paste, Mortar, and Concrete*; ASTM International: West Conshohocken, PA, USA, 2017.
53. ASTM C596. *Standard Test Method for Drying Shrinkage of Mortar Containing Hydraulic Cement*; ASTM International: West Conshohocken, PA, USA, 2017.
54. ASTM C157/C157M. *Standard Test Method for Length Change of Hardened Hydraulic-Cement Mortar and Concrete*; ASTM International: West Conshohocken, PA, USA, 2017.
55. Nematollahi, B.; Sanjayan, J.; Shaikh, F.U.A. Tensile Strain Hardening Behavior of PVA Fiber-Reinforced Engineered Geopolymer Composite. *J. Mater. Civil Eng.* **2015**, *27*, 04015001. [CrossRef]
56. Chi, M.; Huang, R. Binding mechanism and properties of alkali-activated fly ash/slag mortars. *Constr. Build. Mater.* **2012**, *40*, 291–298. [CrossRef]
57. Sood, D.; Hossain, K.M.A. Fresh State, Rheological and Microstructural Characteristics of Alkali-Activated Mortars Developed Using Novel Dry Mixing Technique under Ambient Conditions. *Appl. Sci.* **2021**, *11*, 8920. [CrossRef]
58. Sood, D.; Hossain, K.M.A. Strength, Fracture and Durability Characteristics of Ambient Cured Alkali-Activated Mortars Incorporating High Calcium. *Crystals* **2021**, *11*, 1167. [CrossRef]
59. Nath, P.; Sarker, P.K. Effect of GGBFS on setting, workability and early strength properties of fly ash geopolymer concrete cured in ambient condition. *Constr. Build. Mater.* **2014**, *66*, 163–171. [CrossRef]
60. Pan, Z.; Tao, Z.; Cao, Y.F.; Wuhrer, R.; Murphy, T. Compressive strength and microstructure of alkali-activated fly ash/ slag binders at high temperature. *Cem. Concr. Compos.* **2018**, *86*, 9–18. [CrossRef]
61. Abdollahnejad, Z.; Mastali, M.; Luukkonen, T.; Kinnunen, P.; Illikainen, M. Fiber-reinforced one-part alkali-activated slag/ceramic binders. *Ceram. Int.* **2018**, *44*, 8963–8976. [CrossRef]
62. Korniejenko, K.; Lin, W.T.; Simonova, H. Mechanical properties of short polymer fiber-reinforced geopolymer composites. *J. Compos. Sci.* **2020**, *4*, 128. [CrossRef]
63. Kim, M.S.; Jun, Y.; Lee, C.; Oh, J.E. Use of CaO as an activator for producing a price-competitive non-cement structural binder using ground granulated blast furnace slag. *Cem. Concr. Res.* **2013**, *54*, 208–214. [CrossRef]
64. Askarian, M.; Tao, Z.; Samali, B.; Adam, G.; Shuaibu, R. Mix composition and characterisation of one-part geopolymers with different activators. *Constr. Build. Mater.* **2019**, *225*, 526–537. [CrossRef]

65. Perera, D.S.; Uchida, A.O.; Vance, A.E.R.; Finnie, A.K.S. Influence of curing schedule on the integrity of geopolymers. *J. Mater. Sci.* **2007**, *42*, 3099–3106. [CrossRef]
66. Abdollahnejad, Z.; Mastali, M.; Woof, B.; Illikainen, M. High strength fiber reinforced one-part alkali activated slag/fly ash binders with ceramic aggregates: Microscopic analysis, mechanical properties, drying shrinkage, and freeze-thaw resistance. *Constr. Build. Mater.* **2020**, *241*, 118129. [CrossRef]
67. Adesina, A.; Das, S. Drying shrinkage and permeability properties of fibre reinforced alkali-activated composites. *Constr. Build. Mater.* **2020**, *251*, 119076. [CrossRef]
68. Li, Z.; Liu, J.; Ye, G. Drying shrinkage of alkali-activated slag and fly ash concrete; A comparative study with ordinary Portland cement concrete. *Heron* **2019**, *64*, 149–163.
69. Kuenzel, C.; Vandeperre, L.J.; Donatello, S.; Boccaccini, A.R.; Cheeseman, C. Ambient temperature drying shrinkage and cracking in metakaolin-based geopolymers. *J. Am. Ceram. Soc.* **2012**, *95*, 3270–3277. [CrossRef]
70. Kani, E.N.; Allahverdi, A. Investigating shrinkage changes of natural pozzolan based geopolymer cementpaste. *Iran. J. Mater. Sci. Eng.* **2011**, *8*, 50–60.
71. Sasui, S.; Kim, G.; Nam, J.; Koyama, T.; Chansomsak, S. Strength and Microstructure of Class-C Fly Ash and GGBS Blend Geopolymer Activated in NaOH & NaOH+ Na_2SiO_3. *Materials* **2020**, *13*, 59. [CrossRef]